

AFRL-PR-WP-TR-2006-2226

**ADVANCED FUEL DEVELOPMENT
AND FUEL COMBUSTION**

**Delivery Order 0005: Mitigation of
Particulates Using Fuel Additives**



**M.B. Colket
D.S. Liscinsky
B. True**

**United Technologies Corporation Research Center
411 Silver Lane
East Hartford, CT 06108**

APRIL 2006

Final Report for 15 May 2001 – 18 February 2006

Approved for public release; distribution is unlimited.

STINFO COPY

**PROPULSION DIRECTORATE
AIR FORCE MATERIEL COMMAND
AIR FORCE RESEARCH LABORATORY
WRIGHT-PATTERSON AIR FORCE BASE, OH 45433-7251**

NOTICE AND SIGNATURE PAGE

Using Government drawings, specifications, or other data included in this document for any purpose other than Government procurement does not in any way obligate the U.S. Government. The fact that the Government formulated or supplied the drawings, specifications, or other data does not license the holder or any other person or corporation; or convey any rights or permission to manufacture, use, or sell any patented invention that may relate to them.

This report was cleared for public release by the Air Force Research Laboratory Wright Site (AFRL/WS) Public Affairs Office and is available to the general public, including foreign nationals. Copies may be obtained from the Defense Technical Information Center (DTIC) (<http://www.dtic.mil>).

AFRL-PR-WP-TR-2006-2226 HAS BEEN REVIEWED AND IS APPROVED FOR PUBLICATION IN ACCORDANCE WITH ASSIGNED DISTRIBUTION STATEMENT.

*//Signature//

TIM EDWARDS
Fuels Branch
Turbine Engine Division
Propulsion Directorate

//Signature//

TAMMY KC LOW, Capt., USAF
Deputy Chief, Fuels Branch
Turbine Engine Division
Propulsion Directorate

//Signature//

JEFFREY M. STRICKER
Chief Engineer
Turbine Engine Division
Propulsion Directorate

This report is published in the interest of scientific and technical information exchange, and its publication does not constitute the Government's approval or disapproval of its ideas or findings.

*Disseminated copies will show “//Signature//” stamped or typed above the signature blocks.

REPORT DOCUMENTATION PAGE

Form Approved
OMB No. 0704-0188

The public reporting burden for this collection of information is estimated to average 1 hour per response, including the time for reviewing instructions, searching existing data sources, gathering and maintaining the data needed, and completing and reviewing the collection of information. Send comments regarding this burden estimate or any other aspect of this collection of information, including suggestions for reducing this burden, to Department of Defense, Washington Headquarters Services, Directorate for Information Operations and Reports (0704-0188), 1215 Jefferson Davis Highway, Suite 1204, Arlington, VA 22202-4302. Respondents should be aware that notwithstanding any other provision of law, no person shall be subject to any penalty for failing to comply with a collection of information if it does not display a currently valid OMB control number. **PLEASE DO NOT RETURN YOUR FORM TO THE ABOVE ADDRESS.**

1. REPORT DATE (DD-MM-YY) April 2006		2. REPORT TYPE Final		3. DATES COVERED (From - To) 05/15/2001 – 02/18/2006	
4. TITLE AND SUBTITLE ADVANCED FUEL DEVELOPMENT AND FUEL COMBUSTION Delivery Order 0005: Mitigation of Particulates Using Fuel Additives				5a. CONTRACT NUMBER F33615-97-D-2784-0005	
				5b. GRANT NUMBER	
				5c. PROGRAM ELEMENT NUMBER 62203F	
6. AUTHOR(S) M.B. Colket D.S. Liscinsky B. True				5d. PROJECT NUMBER 3048	
				5e. TASK NUMBER 05	
				5f. WORK UNIT NUMBER EW	
7. PERFORMING ORGANIZATION NAME(S) AND ADDRESS(ES) United Technologies Corporation Research Center 411 Silver Lane East Hartford, CT 06108				8. PERFORMING ORGANIZATION REPORT NUMBER UTRC06-5.100.0037-1	
9. SPONSORING/MONITORING AGENCY NAME(S) AND ADDRESS(ES) Propulsion Directorate Air Force Research Laboratory Air Force Materiel Command Wright-Patterson AFB, OH 45433-7251				10. SPONSORING/MONITORING AGENCY ACRONYM(S) AFRL-PR-WP	
				11. SPONSORING/MONITORING AGENCY REPORT NUMBER(S) AFRL-PR-WP-TR-2006-2226	
12. DISTRIBUTION/AVAILABILITY STATEMENT Approved for public release; distribution is unlimited.					
13. SUPPLEMENTARY NOTES PAO case number: AFRL/WS 06-2464; Date cleared: 17 October 2006. This report contains color.					
14. ABSTRACT The overall technical objective of the program was to develop an additive for JP-8, JP-5, and diesel fuels that will reduce both the mass Emissions Index (grams of PM2.5 emissions/kilogram of fuel) and the number density Emissions Index (particle number density of PM2.5 emissions/kilogram of fuel) in the exhaust of military gas turbine engines by 70 percent. This report summarizes the results of work performed at United Technologies Research Center. Baseline studies were performed with ethanol added to ethylene, as the method and procedures could be validated against the existing experimental database. Experiments were performed in laminar premixed burner-stabilized flat flames. Soot was reduced by factors of about 50% with ethanol. Subsequent tests were performed with mixtures of heptane/toluene/ethylene to provide a better simulation of real fuel chemistry. The most significant effects were observed with a proprietary additive which apparently contains a metal. The use of metals is not perceived to be an environmentally acceptable approach. The next most effective additive is a commercial fuel additive, Kleen, which contains a variety of oxygenated (nitro) compounds. Reductions of soot emissions on the order of 30% were observed. Mixed results were obtained with pyridine, and modeling results show negligible influence of this additive. Finally, advances to a fundamental soot formation model were accomplished by comparing simulations of coflow diffusion flames to experimental data sets. This work resulted in proposed changes to the gas-phase kinetics and soot inception models and identifying the importance of treating soot ageing and radiation losses. The overall goal of identifying an additive that can reduce soot emissions by 70% was not achieved, without use of a metal-containing additive or with very high levels of the additive (>10% by weight). However, advances were made in the understanding or confirmation of (proposed) mechanism for soot formation and will lead to better quantifiable tools for prediction and control of soot emissions during engine design.					
15. SUBJECT TERMS emissions, soot, particulate, gas turbine, additives					
16. SECURITY CLASSIFICATION OF:			17. LIMITATION OF ABSTRACT: SAR	18. NUMBER OF PAGES 66	19a. NAME OF RESPONSIBLE PERSON (Monitor) Tim Edwards 19b. TELEPHONE NUMBER (Include Area Code) N/A
a. REPORT Unclassified	b. ABSTRACT Unclassified	c. THIS PAGE Unclassified			

Table of Contents

Table of Contents	iii
List of Figures	iv
List of Tables	v
Acknowledgements	vi
Summary	1
1. Introduction	2
2. Methods, Assumptions, and Procedures	4
2.1 Experimental Procedures	4
2.1.1 Description of Flat Flame Burners	4
2.1.2 Reactant Flows and Control	6
2.1.3 Measurement Methodology	7
2.1.4 Dilution Probes for Flame Studies	11
2.1.5 Combustor Facility	13
2.2 Modeling Approaches	17
2.2.1 Gas-Phase Chemistry	17
2.2.2 Soot	18
2.2.3 Radiative Power Loss	21
3. Results and Discussions	23
3.1 Experimental Results	23
3.1.1 Selection of Additives	23
3.1.2 Flat Flame Burner Experiments	24
3.1.3 Combustors	34
3.2 Soot Modeling	40
3.2.1 Gas-Phase Kinetics and PAH Chemistry	40
3.2.2 Soot Modeling – Flat Flame	40
3.2.3 Soot Modeling – Well Stirred Reactor	43
3.2.3 Modeling of coflow diffusion flames	49
4. Conclusions	50
References	51
Appendix - Publications/presentations from this work	54
List of Symbols, Abbreviations and Acronyms	55

List of Figures

1. Photograph of the Burner Surface.....	4
2. Flat Flame Facility.....	5
3. Premixed Ethylene / Air Flame at Equivalence Ratio 2.34.....	5
4. Photograph of the Porous Plug Burner.....	5
5. UTRC McKenna Burner.....	6
6. Experimental set-up for the ethanol/ethylene flame experiments.	6
7. Experimental set-up for the heptane flame experiments.	7
8. UTRC Porous-Wall Particle Sampling Probe.....	12
9. Rapid, high-dilution particle sampling system (original concept by Hai Wang).....	12
10. Schematic Diagram of Single-Nozzle-Rig Installed in the Pressure Vessel.....	13
11. Five-Port Probe Installed in the SNR Centerline, With a Diagram of the Port Spacing Shown at Top.....	14
12. View of the Combustor Bulkhead.....	14
13. Single Nozzle Rig Sampling System.....	15
14. Additization Setup for Combustor Experiments.....	15
15. Sampling System used for the Combustor Sector Experiments.	16
16. Internal Design of the Dilution Probe used for Particle Sampling (inlet diameter = 0.066, dilution ratio >10:1)	16
17. Soot Formation Processes in Premixed, Laminar Flame (courtesy of H. Wang).....	19
18. Temperature Along the Centerline of Flame 1 and 2.....	25
19. Soot Volume Fraction via Laser Extinction (LE) and Thermocouple Particle Densitometry (TPD) for Flame 1 and 2.....	26
20. Soot Volume Fractions from Premixed, Laminar Flames. Base Flame is 10% Toluene and 90% Heptane.	27
21. Reduction of Soot in Premixed Flame with Various Levels of Added Pyridine (as ppm in fuel)	28
22. Measured Temperature Profiles for Several Premixed Flames.	30
23. Comparison of Soot Volume Fractions (laser extinction) for Heptane/10% Toluene Flames.	30
24. Relative Soot Production in Laminar Premixed Flame.	31
25. Time Trace Confirming Concentration Effect with Nitropropane.	32
26. Degradation of Diluted Sample (raw signal) due to Orifice Clogging.....	33
27. Particle Size Distributions in Diluted Samples.	33
28. Photomicrographs of Particulates Collected from Premixed Flames using Thermophoretic Sampling.	34
29. Typical Particle Size Distribution in Combustor Experiments.	36
30. Effect of +100 on Median Particle Diameter (diamonds = 240 psia, 900 deg F, triangles = 65 psia, 420 deg F).	36
31. Effect of Pyridine on Median Particle Diameter (diamonds = 240 psia, 900 deg F, triangles = 65 psia, 420 deg F).	37
32. Effect of +100 on Particle Number (diamonds = 240 psia, 900 deg F, triangles = 65 psia, 420 deg F).	37

33. Effect of Pyridine on Particle Number (diamonds = 240 psia, 900 deg F, triangles = 65 psia, 420 deg F).	38
34. Schematic of Hardware and Results for Particle Line Loss Determinations.....	38
35. Penetration Efficiencies of Particulates.....	39
36. Comparison of Predicted Naphthalene With and Without Added Pyridine.....	41
37. Comparison Of Computed Mole Fractions For Several Species As A Function of Height Above The Burner For Fuel-Rich, Premixed Flames With And Without Added Pyridine.	42
38. Normalized Concentrations Of Key Species In Fuel-Rich Premixed Flames With Added Pyridine.	42
39. Predicted Smoke Numbers in PSR Using Two Kinetic Mechanisms for Ethylene and Ethylene with Ethanol Additive.....	44
40. Predicted Temperatures in PSR for Ethylene and Ethylene with Ethanol Additive using the UTRC Kinetic Mechanism.	44
41. Measured Smoke Number as a Function of the Experimental Temperature.....	45
42. Predicted Particle Size Distributions for PSR using UTRC Mechanism.....	45
43. Experimental Particle Size Distribution for Stirred Reactor.	47
44. Computed Penetration Efficiencies of Particles through Sampling Lines.....	49

List of Tables

1. Experimental Test Conditions for the Premixed, Fuel Rich Flames.....	24
2. Percentage Reductions in Soot Volume Fractions in Fuel-Rich Premixed Heptane/Toluene Flames due to Presence of Various Fuel Additives.....	28
3. Mixture Mole Fractions and Fuel Mass Fractions for Premixed Flames.....	29
4. Particle Reduction Effectiveness of Kleen Components ($\phi = 2.4$).....	31
5. Test Conditions for Combustor Sector Testing.....	35
6. Efficiency for Transport of Particles through Sample Line without Diffusional Loss to Walls (5 lpm, 0.18" ID tube, 293K, 1 atm).....	48

Acknowledgements

This program probably would not have happened with the leadership and inspiration provided by Dr. Mel Roquemore, nor without the technical guidance of Prof. Tom Litzinger. We are highly indebted to both of these individuals. In addition, the expertise and team coordination and contributions from Profs. Bob Santoro and S. Sidhu and Drs. Scott Stouffer, Vish Katta, Edwin Corporan, and Kevin McNesby are gratefully acknowledged. Also, the collaborations with Profs. Mitch Smooke and Marshall Long and with Dr. Bob Hall continue to result in high value research, and we very much appreciate their collective and individual efforts. Finally, the program coordination by Drs. Don Phelps and Halny Pawlik are gratefully appreciated, as is the patience of Dr. Tim Edwards.

Summary

There is a growing body of evidence that small soot particles cause both health and environmental problems. Hence, this effort was directed towards reducing particulate emissions from gas turbine engines. The project was linked to a joint DoD, industry, and university program supported by the Strategic Environmental Research and Development Program (SERDP PP1179) that was focused towards reducing particulate emissions by modification of the fuel through the use of fuel additives. The overall technical objective of the program was to develop an additive for JP-8, JP-5, and diesel fuels that will reduce both the mass Emissions Index (grams of PM_{2.5} emissions/kilogram of fuel) and the number density Emissions Index (particle number density of PM_{2.5} emissions/kilogram of fuel) in the exhaust of military gas turbine engines by 70 percent. This report summarizes the results of work performed at United Technologies Research Center.

Baseline studies were performed with ethanol added to ethylene, as the method and procedures could be validated against the existing experimental database. Experiments were performed in laminar premixed burner-stabilized flat flames. Soot was reduced by factors of about 50% with ethanol. Subsequent tests were performed with mixtures of heptane/toluene/ethylene to provide a better simulation of real fuel chemistry. The most significant effects were observed with a proprietary additive which apparently contains a metal. The use of metals is not perceived to be an environmentally acceptable approach. The next most effective additive is a commercial fuel additive, Kleen, which contains a variety of oxygenated (nitro) compounds. Reductions of soot emissions on the order of 30% were observed. Mixed results were obtained with pyridine, and modeling results show negligible influence of this additive.

Detailed chemical kinetic modeling supported the above experiments, but also was used to explain some unusual results obtained in the well-stirred reactor experiments using ethanol as an additive to ethylene combustion. In particular, a slight increase in soot emissions with added ethanol was explained through the dependence on temperature. In modeling these stirred reactor results, a modified code was used that fully couples the chemical kinetics and soot aerosol dynamical equations into a stirred reactor code. As part of this work, advances and demonstrations of technologies for the accurate collection of soot particles were accomplished, including probe design, sample system performance, and diagnostics.

Finally, advances to a fundamental soot formation model were accomplished by comparing simulations of coflow diffusion flames to experimental data sets. This work resulted in proposed changes to the gas-phase kinetics and soot inception models and identifying the importance of treating soot ageing and radiation losses.

The overall goal of identifying an additive that can reduce soot emissions by 70% was not achieved, without use of a metal-containing additive or with very high levels of the additive (>10% by weight). However, advances were made in the understanding or confirmation of (proposed) mechanism for soot formation and will lead to better quantifiable tools for prediction and control of soot emissions during engine design.

1. Introduction

This effort is linked to a joint Army, Navy, Air Force, and University program supported by the Strategic Environmental Research and Development Program (SERDP PP1179) that addresses particulate emissions from turbine engines in aircraft, helicopters, ships, and tanks. There is a growing body of evidence that small soot particles cause both health and environmental problems; this work is focused towards reducing those emissions by modification of the fuel through the use of fuel additives. The overall technical objective of the program is to develop an additive for JP-8, JP-5, and diesel fuels that will reduce both the mass Emissions Index (grams of PM_{2.5} emissions/kilogram of fuel) and the number density Emissions Index (particle number density of PM_{2.5} emissions/kilogram of fuel) in the exhaust of military gas turbine engines by 70 percent.

The EPA considers PM_{2.5} an important air pollutant because these small particles can penetrate deep into the lungs and cause significant health problem. In 2005, the EPA proposed revisions to The National Ambient Air Quality Standards (NAAQS) that would reduce the PM_{2.5} 24-hour standard from 65 $\mu\text{g}/\text{m}^3$ to 35 $\mu\text{g}/\text{m}^3$. This could pose problems for DoD airbases since the major source of PM_{2.5} emissions produced by the DoD is gas turbine engine powered aircraft. In 2004, DoD aircraft produced about 4.2×10^{10} kg of PM_{2.5} emissions. Much of these emissions occur in local areas around active airbases. If an airbase is in a region that is non-compliant with the PM_{2.5} NAAQS, then by law the base has to comply with the state implementation plan (SIP) to bring the region into compliance with the local air quality standards. Thus, the SIP can indirectly regulate PM_{2.5} emissions from military aircraft leading to adverse effects on aircraft basing and military activities. DoD has experienced this type of problem in the past related to NO_x emissions from military aircraft operating from bases in non-compliant regions. The EPA is currently identifying the PM_{2.5} non-compliant regions, which could cause similar problems for military bases in non-compliant regions.

This work addresses the use of additives for reducing soot emissions from gas turbine powered aircraft.

The key to improving the predictability of the formation of all particulate matter below 2.5 micrometers (PM_{2.5}) in DoD gas turbine (and diesel engine) combustors is an improved understanding of the chemical and physical fundamentals involved in particle nucleation, growth, and oxidation. Improvement of the knowledge base of the formation and reaction mechanisms of polycyclic aromatic hydrocarbons (PAH) is essential to improving that understanding. Many other important computational and analytical skills are also involved in the translation of that fundamental knowledge into computational procedures useful for predicting soot formation for a variety of DoD gas turbine and diesel engine environments and fuel types.

The role of United Technologies Research Center (UTRC) in achieving these objectives has been to perform fundamental experiments investigating the effect of additives on soot growth in fuel-rich flames, and aeroengine combustors. Furthermore, UTRC participated

in interpretation of these data as well as data obtained by other program participants using detailed flame models and soot formation codes.

The work described herein is focused primarily on work performed at UTRC, although this project was part of a much larger team investigating the ability of fuel-additives to mitigate the soot emissions from aircraft engines. Prior work has been performed in this area, but often the works had conflicting conclusions, with no clear answer as to whether an additive had a positive or negative effect on reducing soot. To minimize such complications, this team adopted a comprehensive approach, by investigating the effect of a single additive on the formation of soot in many different experimental environments, including shock tubes, stirred reactors, premixed laminar flames, opposed-jet diffusion flame, turbulent flames (atmospheric pressure and elevated pressure), and gas turbines. A variety of diagnostic methods were employed. This detailed experimental work was supported with a variety of computational modeling techniques that included detailed chemical kinetics, PAH modeling, and soot formation submodels. In addition some work was done modeling coflow flames to enhance the detail modeling capabilities of soot formation.

In addition to UTRC, the team members included staff from Pennsylvania State University (PSU), Army Research Laboratories (ARL), the University of Dayton Research Institute (UDRI), and Air Force Research Laboratories (AFRL). In addition, the University of Missouri, Rolla (UMR) also supported the early phases of the program. This program was coordinated with a companion SERDP-funded program

The initial focus of the work was to validate the methods and procedures by investigating the effect that ethanol has on reducing soot in ethylene flames. This chemical system was selected since substantial work has been performed on soot formation in ethylene flames, ethylene kinetics, and the use of ethanol for reducing soot. While these efforts were proceeding, AFRL was scanning a large number of fuel-additives in a gas turbine environment to help point the direction of subsequent work. This work identified a commercial additive. Kleen, normally used in the racing car industry. Hence the later phase of the project was focused on testing Kleen and its components. In addition, significant efforts were spent on investigating the use of pyridine for which some encouraging results had recently been observed.

2. Methods, Assumptions, and Procedures

The majority of the experiments at UTRC were performed using a premixed, laminar flat flame facility, although substantial changes to the experimental hardware occurred during this program. These changes included modifications to the burner hardware, additive injection systems, and particulate sampling system. In addition, measurements were made by piggybacking on tests in the Jet Burner Test Stand at UTRC for model combustors and at the Pratt and Whitney x960 test for annular rig tests of main aeroengine combustors, although additive tests were not performed at x960. Limited modeling was performed for the premixed laminar flames and to support companion studies on the stirred reactor. Also, the kinetics models were enhanced at UTRC and shared with team members. Finally, limited work was performed in collaboration with colleagues from Yale to support refinements to our existing soot model, based on comparison to existing data sets on soot formation in coflowing flames.

2.1 Experimental Procedures

2.1.1 Description of Flat Flame Burners

Experiments were initiated in 2001 using a flat flame burner as shown in Figure 1. The perforated surface of the Hastalloy burner consists of 513 holes which are 1mm in diameter arranged as a regular octagonal. This design was utilized to avoid potential problems associated with coking and reaction within narrow passages in conventional porous plug burners. The laminar flame is stabilized using a 20 cm diameter ceramic plate located 30 mm above the burner surface and by using an argon coflow. The facility is partially shown by the photo in Figure 2 with a close-up of the flame shown in Figure 3. Open area of the 513 holes is 4.0 cm^2 and the effective burner area is estimated to be 19.6 cm^2 .

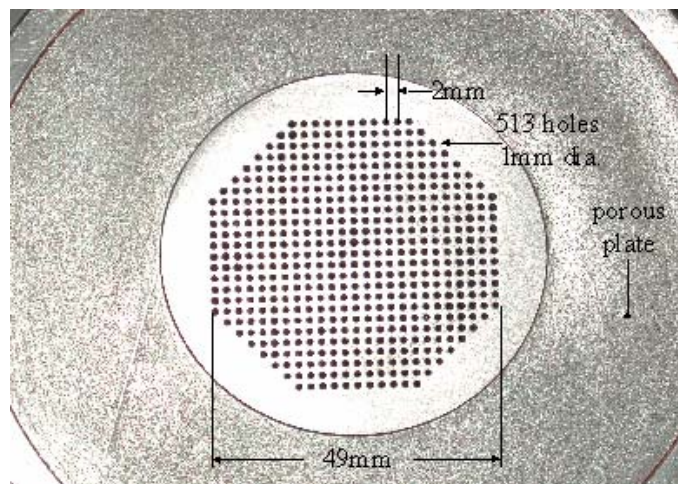


Figure 1. Photograph of the Burner Surface

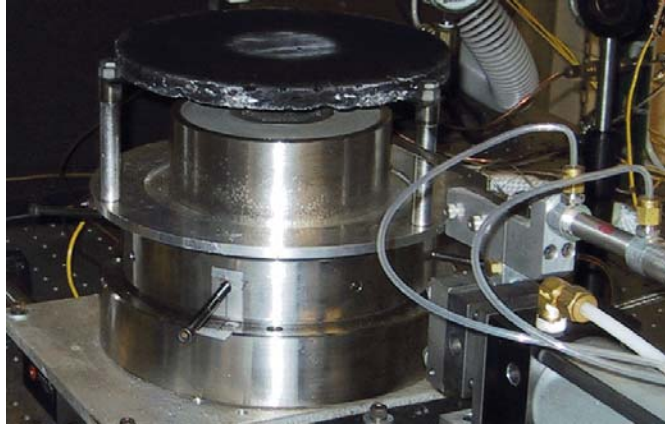


Figure 2. Flat Flame Facility



Figure 3. Premixed Ethylene / Air Flame at Equivalence Ratio 2.34

In 2002, the burner surface was changed to a porous plug due to concerns that jetting was creating localized non-uniformities in the flame. The burner surface is shown in Fig. 4.

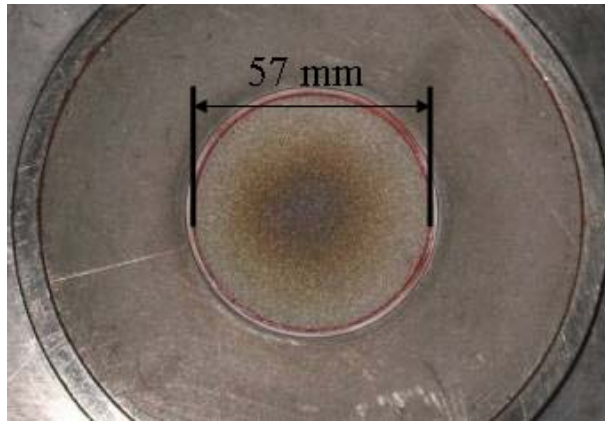


Figure 4. Photograph of the Porous Plug Burner Used from 2002 to September 2005

In 2005 a McKenna burner was deployed at UTRC to more closely match test conditions being used at PSU. A photo of the burner and flame is shown in Figure 5.



Figure 5. UTRC McKenna Burner

2.1.2 Reactant Flows and Control

Control of reactant gas and coflow to the premixed burner was performed using Brooks 5800 series massflow controllers which were calibrated using wet-test meters prior to use. The additives were introduced (along with the reactants) into a 1L vaporization /mixing chamber maintained at 200C. The mixing chamber was connected to the base of the burner with 50 cm of 6.35mm OD heated stainless steel tubing. Initially the introduction of the liquid additives (ethanol) was performed using concentric, high flow, high efficiency, Meinhard Nebulizers (HEN model). Calibration of the borosilicate nebulizers showed that liquid delivery vs flow (and pressure) was highly reproducible and that a stream of fine droplets was produced. By introducing the stream of fine droplets into the heated chamber, vaporization and mixing with the reactants was achieved.

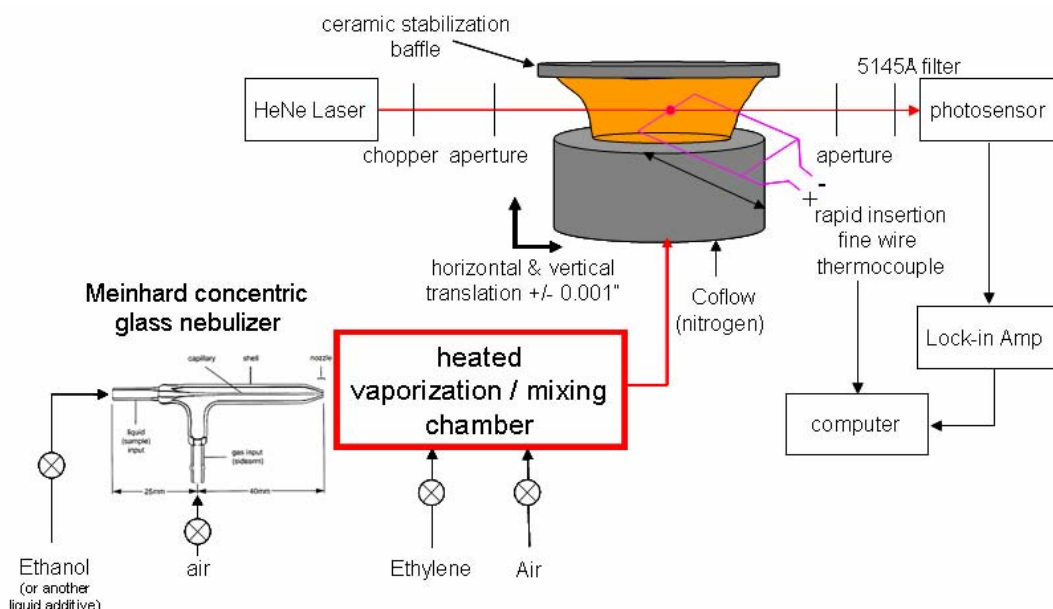


Figure 6. Experimental set-up for the ethanol/ethylene flame experiments.

Although the nebulizers worked well, more flexibility is afforded by use of high pressure syringe pumps, especially for experiments with liquid fuel, i.e. heptane – toluene

mixtures. Two ISCO 500D precision syringe pump systems were installed which allowed on-demand control of fuel and additive(s) at any given flowrate from 0.001 to 200 ml/min. Delivery flowrates were verified to be better than 1% of setpoint by experiment. The additives and fuel were mixed with air and introduced into the heated vaporization chamber.

2.1.3 Measurement Methodology

During this program four different methodologies were used to characterize soot evolution in the premixed flat flames with respect to: (1) particle size distribution, (2) particle number concentration, and (3) particle morphology. A brief discussion of each of experimental methods follows:

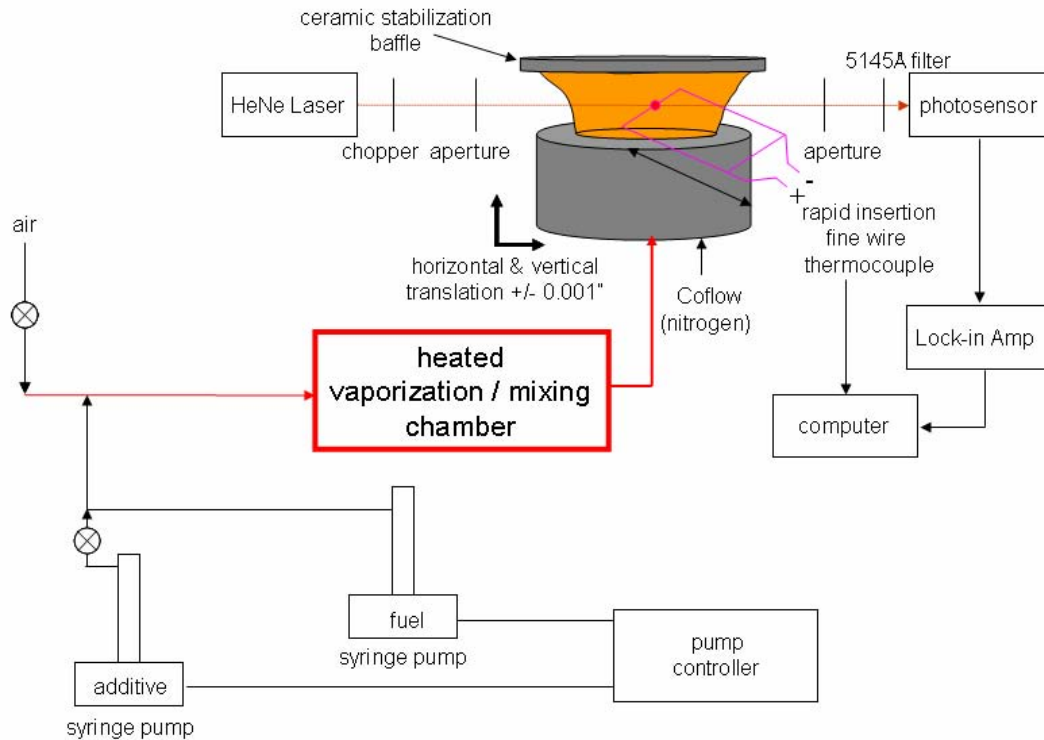


Figure 7. Experimental set-up for the heptane flame experiments.

(1) Thermocouple Particle Densitometry (TPD)

Soot volume fraction was measured using temperature particle densitometry (TPD). The technique, described in detail by McEnally et al. (1997), consists of rapid insertion of a thermocouple into the flame and recording the junction temperature (T_j) as a function of time. The T_j history responds to soot deposition that consists of a transient-response stage (0 – 0.2s), a variable-emissivity stage (0.2 – 5s) and a variable-diameter stage (>5s). T_{jo} obtained from a linear extrapolation of the temperature history to time zero and then corrected for radiation to obtain gas temperature (T_g) by calculating a heat balance:

$$\epsilon_j \sigma T_{jo}^4 = (k_{go} Nu_j / 2d_j) (T_g^2 - T_{jo}^2) \quad (1)$$

The thermophoretic mass transfer model used by McEnally was used to calculate the local soot volume fraction. The slope of a linear fit to the temperature history in the variable diameter stage is proportional to the soot volume fraction:

$$m = \beta f_v \quad (2)$$

where,

$$\beta = 2D_T \epsilon_j \sigma^2 T_s^4 / (\phi k_{go}^2 Nu_j) \quad (3)$$

Note that a thermophoretic model can be used since particles <1µm will not deposit on the bead by inertia but rather follow the gas streamlines. Furthermore Rosner et al., 1991 have shown that Brownian diffusion is small relative to thermophoresis.

The thermocouple assembly also follows that of McEnally in that the bead is stretched (to avoid sagging) between two supports that are 50mm apart (to avoid conduction losses). Uncoated type R thermocouples (Pt-Pt/13%Rh) of several spherical bead sizes (0.165 to 0.203 mm) as well as butt-welded 0.076 mm beads were used. The assembly was driven pneumatically and the data acquisition system was triggered optically to begin recording with thermocouple insertion times being less than 100ms. Datapoints were recorded at 200Hz for 40 seconds using LabView[®] to sample an I/O interface card (National Instruments AMUX-64T) that has an integrated circuit temperature sensor and electronic cold junction compensation, i.e. thermocouple inputs.

One of the parameters used in the calculation of f_v is the soot deposit solid fraction (ϕ), or void fraction. Soot deposit density for the flame was obtained by collecting soot on a Pt wire. The weight and diameter of the wire was determined before the experiment and after collecting the soot. Knowing the volume and mass of the soot, the density of the deposited soot particles could be calculated. ϕ is the ratio of the soot deposit density to the material density of soot (1.8 g/cc). In the post flame front regions of both flames ϕ was measured to be 0.013 (\pm 0.001).

3. *Laser Extinction (LE)*

Laser extinction is widely used to measure soot volume fraction (f_v) in flames because of its simplicity and non-intrusive nature. Number density (N) is derived from the measured light incident on (I_o) and transmitted through the flame (I), the extinction cross section (σ_e) and extinction pathlength (L) which are related by Beer's law:

$$I = I_o(\exp(-N\sigma_e L)) \quad (4)$$

A schematic of the laser extinction setup used for this work is shown in Fig. 6. A cw Spectra-Physics 10mW HeNe laser (632.8 nm) was used as the light source for the extinction measurements because of its good stability and low noise characteristics. Variable diameter apertures located 10cm from the burner centerline on either side of the burner were used to reject diverging beams and forward scattered light. Typically the laser side aperture diameters was less than 1mm and the detector side aperture diameter was 5mm. After passing through the flame the light was collected by an integrating sphere that ensured that the measured transmitted intensity was not affected by changes in beam direction due to beam steering. The light intensity was measured with a

photodiode (Newport 818SL) after passing through a narrow-band optical filter (12nm) to reduce broadband flame radiation and an OD 3 neutral density filter to prevent saturation of the sensitive detector. Although suitable measurements can be made without signal processing, signal-to-noise ratio can be improved by removing practically all flame emission with the addition of a mechanical chopper (Ithaco model 220) and lock-in amplifier (Stanford Research model SR510). A modulation frequency of 400 Hz was used.

To calculate f_v the extinction coefficient must be known in addition to the light intensities. The extinction coefficient depends on the complex refractive index (n) and wavelength of the incident light (λ):

$$\sigma_e = 6\pi E(n) f_v / \lambda \quad (5)$$

where,

$$E(n) = -\text{Im}(n^2 - 1) / (n^2 + 2) \quad (6)$$

Rayleigh theory for small particles ($d_p \ll \lambda$) was applied to relate absorption to volume fraction. Although it will be seen that high in the flame chains of agglomerates are not in the Rayleigh range, theory shows that the absorption is simply the sum of the primary particles regardless of whether they are isolated or agglomerated (Berry and Percival, 1986). As long as the primaries are in the Rayleigh range the effect of agglomeration is small (1.8% or less) as has been shown by Charalampopoulos and Chang (1991). Since transmission is a relative measurement, the extinction coefficient requires no calibration, however the pathlength must be known and homogeneous. For each flame σ_e was determined at several heights using tomographic reconstruction to deconvolve the local soot absorption coefficient from a set of parallel measurements of transmission. Each dataset consisted of 60 measurements spaced at 1mm intervals starting over the coflow and progressing toward the centerline of the burner. Finally, a soot refractive index (n) of $1.57 - 0.56i$ (Dalzell and Sarofim, 1969) was used although there is some range to the values reported in the literature ($1.90 - 0.55i$ (Lee and Tein, 1982)). Therefore:

$$f_v = -\ln(I/I_0) \lambda / 6\pi E(n)L \quad (7)$$

4. *Transmission Electron Microscopy (TEM)*

When particles that are small with respect to the gas mean free path are exposed to a significant temperature gradient, the particles move in the direction of decreasing temperature with a velocity that is independent of particle diameter (Waldman and Schmitt, 1966) and morphology (Rosner, et.al., 1991). Therefore insertion of a cold surface into the flame results in soot deposition by thermophoresis. Methodology developed by Dobbins and Megaridis (1987) was used to perform thermophoretic sampling. Specifically a computer controlled two-stage sampling system was built using bi-directional pneumatic cylinders (Bimba Manufacturing) and fast acting solenoids. The first cylinder positioned the probe assembly in the flame, while the second cylinder deployed a thin probe holder to collect the sample. The sample is collected onto a standard 3mm diameter carbon coated microscope grid (Ted Pella Inc., pn 01810 – 200 mesh copper grid and 20nm thick carbon substrate) which was protected in a sheath during the first stage of insertion. The grid was exposed to the flame for 10 to 40 ms before retracting into the sheath and withdrawing from the flame. The entire sampling

sequence generally required less than 400ms with the timing chosen so that soot coverage of the grid was about 10%. A two-stage system was built to allow short exposure (sampling) times while minimizing flame disturbances. Although intrusive, this extractive technique preserves particle morphology since the cold surface stops heterogeneous reactions of the particles as they are captured.

The grids obtained by thermophoretic sampling were analyzed by bright field transmission electron microscopy (TEM). Photomicrographs were made at magnifications up to 100,000X on a Philips EM 400. Computer assisted image analysis (NIH Image) provided measurement of soot primary particle diameter (d_p) and morphology. This analysis is made tedious by the minimal contrast between the background (the carbon substrate) and the soot. In addition the edges of the particles tend to be amorphous and therefore not sharply defined. Several characteristic dimensions can be obtained from these photomicrographs. The first is the primary particle diameter (d_p). This measurement is straightforward. The second is L_{max} or Feret's diameter. This is the maximum distance between any two points on the perimeter of an agglomerate. These two parameters can be used to calculate the number of primary particles per agglomerate (N_p) were estimated using an empirical relation reported by Megaridis, 1990:

$$N_p = k_f (L_{max}/d_p)^{D_f} \quad (8)$$

where k_f is a prefactor and D_f a fractal dimension that accounts for the 3-dimensional shape of the agglomerate, i.e. "compactness" (values of from 1.62 to 1.85 have been reported).

5. Differential Mobility

Electrostatic forces are commonly used to separate particles. Since the electrical mobility of a particle can be accurately calculated, particle size and particle distribution can be measured using electrophoresis. This approach is particularly effective for spherical particles with submicrometer diameters. An electrostatic classifier (TSI 3071) and a condensation nucleus counter (CNC, TSI 3022) were used with a dilution probe to obtain soot size distributions in the 10 to 500 nm size range (Fig. 9). The classifier separates particles by their drift in an electric field. The velocity a particle acquires is a function of size and charge. After an impactor removes particles greater than 1 μ m and a radioactive source "neutralizes" all particles (ensured that they have equilibrium distribution of charges), a known size range of particles can be selected by choice of electric field and instrument flow parameters. The particles are detected using the CNC which uses a supersaturated vapor that can condense on the particles to form droplets that can be counted optically. The instrument is operated in a scanning mode so that a complete size distribution can be acquired in as little as 60 seconds. The combination of the classifier and CNC operated in a scanning mode is referred to as a scanning mobility particle sizer (SMPS).

Based on the drift time through an electric field, the classifier separates particles based on their 'aerodynamic' diameter, d_{aero} , which is the equivalent diameter of a spherical particle drifting through the field. For an irregularly shaped particle such as soot agglomerates, this parameter in general is not identical to any fundamental parameter of the agglomerate. As a preliminary means of interpreting size information provided by the

SMPS, we recognize (Willeke and Baron, 1993) that $d_{\text{aero}} = \chi d_{\text{ev}}$, where d_{ev} is the equivalent volume diameter and χ is the dynamic shape factor. Furthermore, we have derived an approximate expression:

$$L_{\text{max}} = A(d_p)^a (d_{\text{aero}}/\chi)^b \quad (9)$$

based on the relationships developed by Koylu, et al. L_{max} is Feret's diameter as discussed previously. We utilize a value of 1.7 for χ and have determined constants A, a, and b in order to enhance the comparison between our SMPS and TEM results. Values of d_p are extracted from the TEM results to reduce the data. No information is provided from the SMPS to assess whether or not a particle is a single (nearly spherical) particle or a complex aggregate. Hence, we have also adopted simple algorithms to transition the values of the constants to appropriate numbers to ensure that the above equation reduces to $L_{\text{max}} = d_p$ for a single particle. Using this procedure and expressions provided by Koylu, et al., we are then able to compute distributions of L_{max} , and N_p , as well as N and f_v using d_p from the TEM and the distributions from the SMPS:

$$f_v = \pi/6 d_p^3 \sum N_p (300/T_g) \quad (10)$$

To use the SMPS, samples were extracted from the flame using a stainless steel dilution probes (Figs. 8 and 9). The inner wall of the probe was a 0.125" ID porous tube. The probe was operated at a water temperature of ~90F. Nitrogen dilution was metered to the probe and sample was drawn into the probe using an eductor instead of a pump. The motive flow added a second stage of dilution. Dilution rate was determined by online monitoring of CO and conditions were set to be isokinetic at the probe entrance before initiating data collection.

2.1.4 Dilution Probes for Flame Studies

Extraction of particle samples from the premixed flame requires rapid dilution to avoid particle coagulation and water condensation. These two sample transport factors can drastically alter measured particle size distributions. In addition particle concentrations are generally too high for direct measurement with standard instrumentation such as a differential mobility analyzer, as particle-particle collisions rapidly alter the size distribution at high number densities. Three different dilution probes were used with during the premixed flame experiments. The first was briefly described in the previous section when the differential mobility methodology was discussed. A second probe, as shown in Fig. 9, was deployed in a prior effort at UTRC (Colket, et al, 2001). This probe has a porous wall and can provide high dilution ratios but suffers in that the water cooling near the tip thermophoretically collects particles on the wall of the sample tube which tends to choke the flow as particles deposit. A variety of operational issues, however, make this probe awkward to use, with no guarantee of rapidly freezing the particle size distribution.

A more reliable probe design for high dilution and small particle sampling is one described in detail by Zhao, et al (2003, 2005). We deployed the probe in a similar

fashion to that described in the literature as shown in Fig. 9. In this sampling system a 1/4" diameter stainless steel tube with a 0.007" machined (EDM) hole was placed horizontal to the burner with the hole facing the flow. Nitrogen is metered into the tube and exhausted with a pump. By monitoring the pressure differential sample could be drawn into the nitrogen flow and dilution ratios of 1000 or higher could be achieved. This probe/sampling system was found to work well at flame stoichiometries near the on set of sooting, however it was difficult to operate the system for extended periods at equivalence ratios of interest, ie 2.5. Still samples could be obtained for on the order of 10min before the orifice clogged.

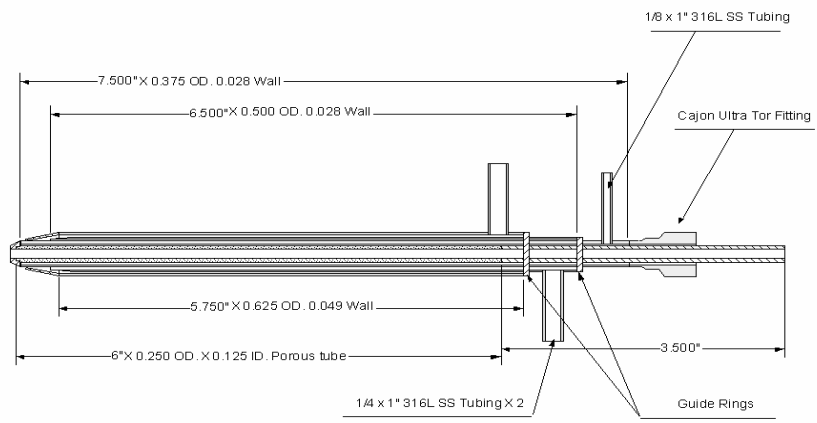


Figure 8: UTRC Porous-Wall Particle Sampling Probe

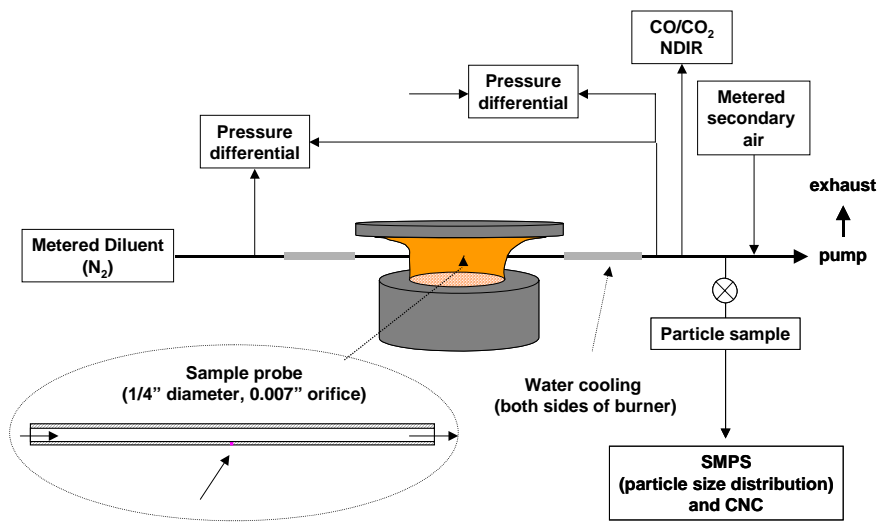


Figure 9: Rapid, high-dilution particle sampling system (original concept by H. Wang)

2.1.5 Combustor Facility

Additive experiments were performed in a moderate pressure and temperature single nozzle rig (SNR). This combustor was located in the Jet Burner Test Stand at UTRC. The nozzle is installed in a plenum-fed pressure vessel on the centerline, as shown in the schematic diagram in Figure 10. The combustor was nominally 4" by 4" and had convectively-air-cooled side walls. The dilution hole patterns were located on the top and bottom walls of the combustor. The fuel injector was mounted in the front of the combustor. A five-port traversing probe was available to extract samples from the combustion gases (see Figure 11). This probe was located at the combustor exit. The probe was oriented such that samples were acquired along the midplane of the combustor that was parallel to the OD and ID liners containing the combustion air holes. The samples from each port were ganged together to represent an area-averaged sample at the exit plane of the combustor. The combustor is shown in Figure 12.

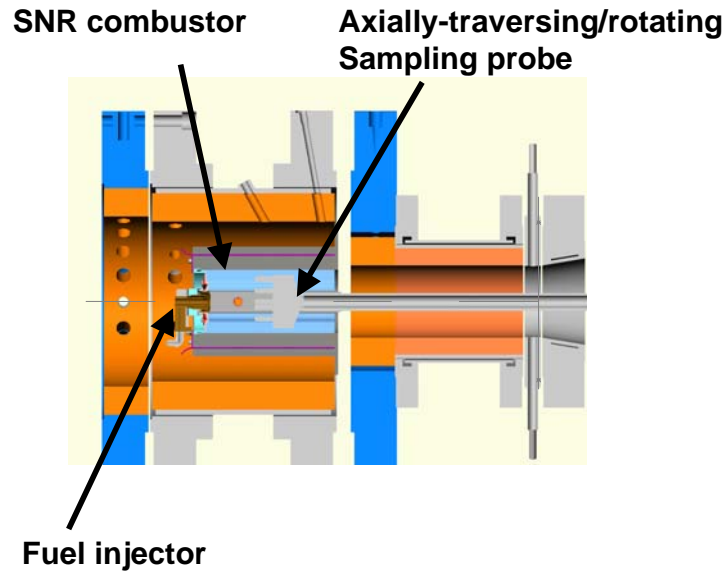
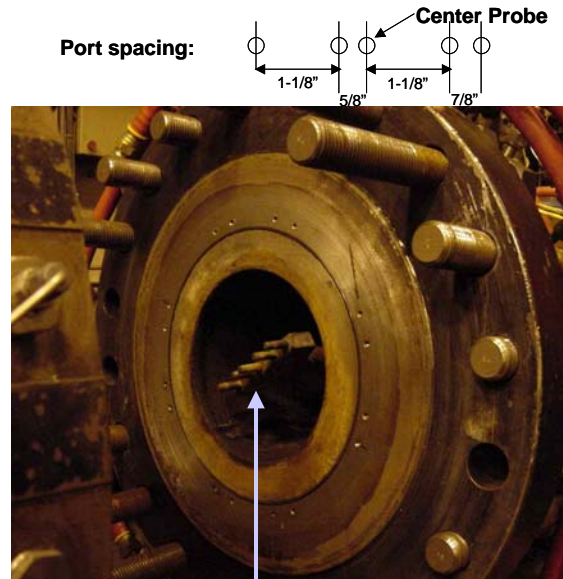
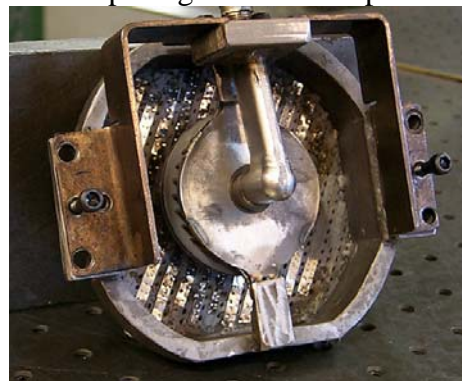


Figure 10. Schematic Diagram of Single-Nozzle-Rig Installed in the Pressure Vessel



Probe is oriented 36-deg. from horizontal axis.
 Combustor is also oriented the same, with the OD panel on top.

Figure 11. Five-Port Probe Installed in the SNR Centerline, With a Diagram of the Port Spacing Shown at Top.



View Looking from Upstream

Figure 12. View of the Combustor Bulkhead

The sampling system is shown schematically in Figure 13. Samples are acquired at the combustor exit and diluted with N₂ downstream for transport to the particle measurement instrumentation. Measurement of CO₂ is used to determine dilution ratio. In addition to smoke number, particle size distributions were determined using a scanning mobility particle sizer (describes in section 2.1.3). Sample were also collected using an Anderson Impactor with subsequent inspection of the filter media using Scanning Electron Microscopy.

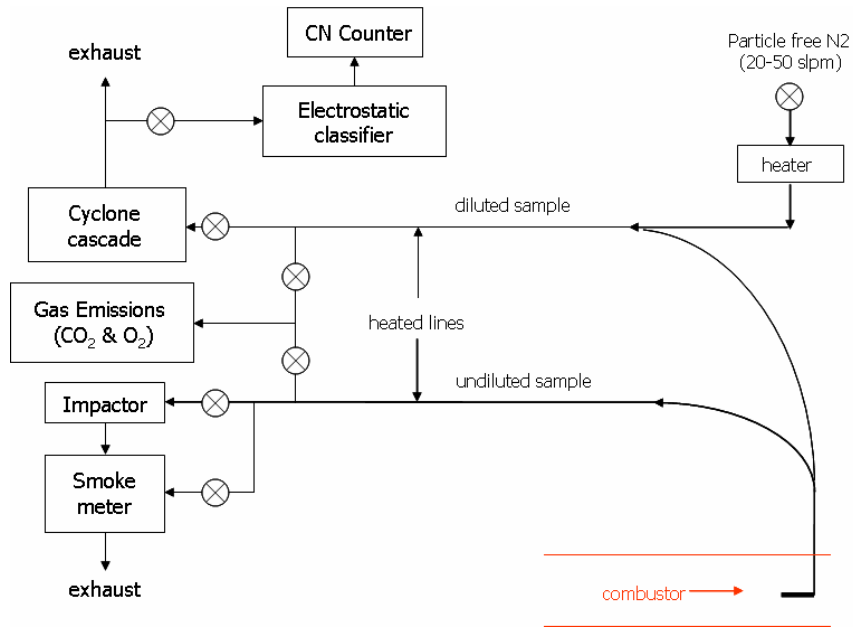


Figure 13. Single Nozzle Rig Sampling System.

Previous experiments using this combustor provided results which were reported in AIAA-2001-3745. In those experiments a military style nozzle and dilution air was modified to ensure soot production. Also additization was performed by batch-mixing the fuel and additives in 55 gallon drums prior to use. In this program additization was performed using syringe pumps as shown in Figure 14. The advantage of the syringe pumps is precise metering with the ability to quickly turn the additive off and on as well as change additive concentration.

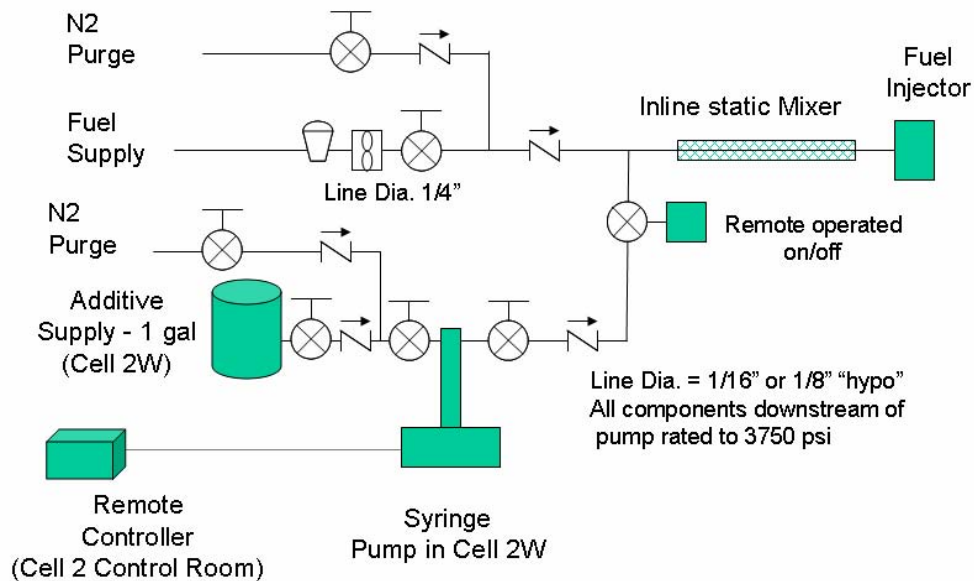


Figure 14. Additization Setup for Combustor Experiments

The SNR experiments were performed first using a commercial style nozzle. The previous experiments, where batch-mixing was used, used a military nozzle. So a second set of experiments were also performed using a military-style nozzle.

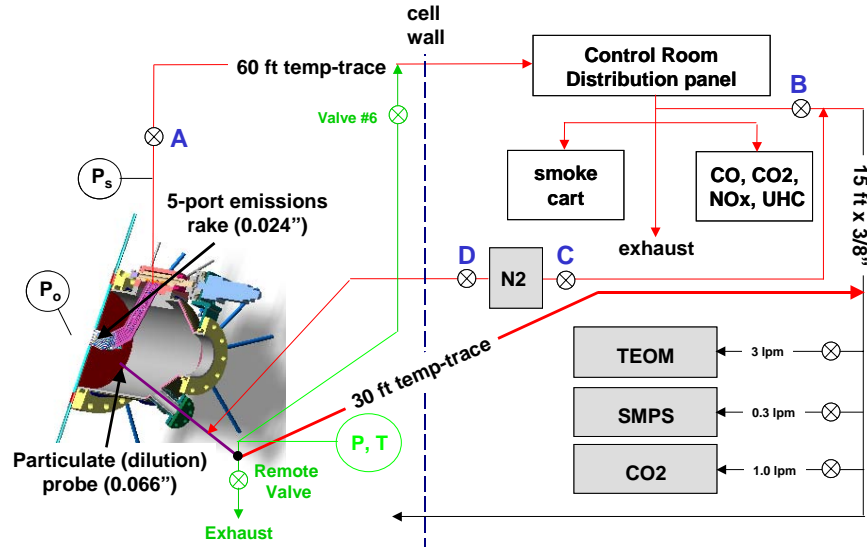


Figure 15. Sampling System used for the Combustor Sector Experiments.

A second combustor was also used of additive experiments. This combustor was a 4-nozzle sector shown schematically along with the sampling system in Figure 15. A standard gas sampling probe rake is able to traverse the sector. In addition to the gas probe, particle samples were acquired using the sampling system shown in Fig. 15 with a water-cooled dilution probe specially suited for particulate sampling. The two probes could not be used simultaneously, however the gas probe can be parked near the particle probe. Sample dilution at the probe tip can be shown to (help) preserve particle size distribution. The internal geometry of the probe is shown in Fig. 16. The probe was located at the midpoint of the combustor sector and was stationary during testing. For the reported results the probe was operated with an 11:1 dilution ratio.

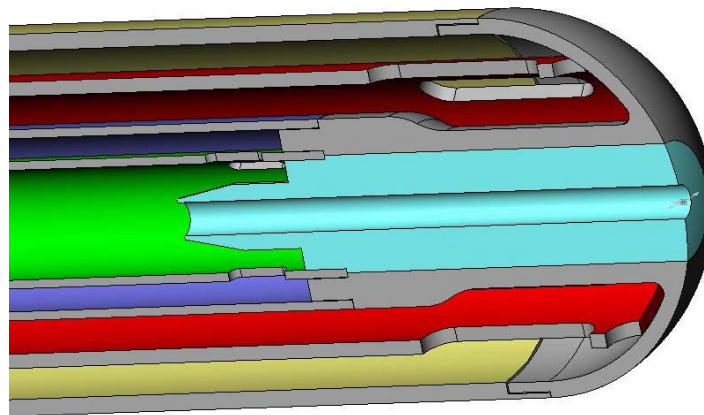


Figure 16. Internal Design of the Dilution Probe Used for Particle Sampling (inlet diameter = 0.066, dilution ratio >10:1)

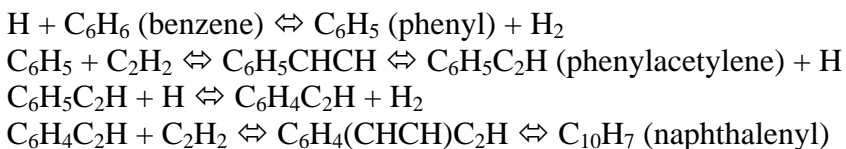
2.2 Modeling Approaches

2.2.1 Gas-Phase Chemistry

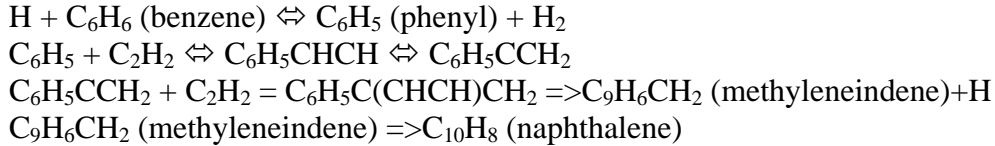
To support the kinetics modeling throughout the program, UTRC has created reduced versions of the large heptane-based chemical kinetic mechanism developed at NIST under a companion SERDP program. This mechanism has also been extended and utilized by team members to evaluate the impact of the addition of nitroalkanes. In addition, a chemical kinetics submodel for the pyrolysis and oxidation of pyridine has been developed and added to the reaction set for heptane.

Aromatic rings participating in the soot inception and soot growth steps can be either formed from cyclization of lower molecular weight hydrocarbons, produced from dehydrogenation of cycloalkanes, or provided by the parent fuel. It is now believed that for many flames, the dominant step is initiated by either propargyl radical recombination or $C_3H_3 + C_3H_4$ [Colket and Seery, 1984, Wu and Kern, 1987] to form benzene or phenyl radical through a complex rearrangement pathway [Melius, et al, 1993]. Hence, processes leading to the formation of C_3H_3 and C_3H_4 can be the bottleneck to ring and hence soot formation – and quantitative prediction of these species is perceived to be a prerequisite to quantitative modeling for laboratory flames. It is worth noting that, while the rate coefficients for these steps are now established probably to within a factor of two, there are still uncertainties in the pathways that govern the formation and destruction of such critical species. Other steps, initiated by C_2H_2 addition to *n*- C_4H_5 or to *n*- C_4H_3 may contribute [Colket, 1986; Frenklach, et al, 1985], as well as reactions involving cyclopentadienyl moieties [Marinov, et al, 1998]. Questions about the importance of the ‘normal’ variety of C_4H_3 or C_4H_5 radicals with the radical sites on the end carbons have been raised for some time as these isomers are strongly disfavored thermodynamically and recent measurements confirm these concerns [Hansen, et al, 2006]. Hence, Colket and Westmoreland [2006] have argued about possible roles of *i*- C_4H_5 and *i*- C_4H_3 in ring formation.

Modeling the formation of multi-ring aromatics is more challenging, with few quantitative demonstrations of such simulations. The preferred reaction pathway is



although several other reaction pathways (involving toluene/benzyl and indene/indenyl [Colket and Seery, 1994] or cyclopentadiene/cyclopentadienyl dimerization [Marinov, et al, 1998, for example] have been proposed. In addition there are discussions [Colket and Westmoreland, 2006] involving the role of species such as $C_6H_5CCH_2$, such as:



2.2.2 Soot

Quantitative modeling of particulate matter (PM), often referred to as soot or smoke, emissions from flames is one of the greatest challenges to computational modeling of combustion. First, formation of PM itself is an incompletely understood process. However, there exists models that provide quantitative predictions of laboratory flames burning pure fuels at atmospheric pressure, but generally they are accurate over very limited conditions. Second, oxidation of these particles is dependent on accurate knowledge of the active surface area of the particles which in turn is dependent on the formation process. Third, the total emissions of PM from a practical burner are the difference between two large terms, the formation and the oxidation. At full power for example, PM emissions can be two to three orders of magnitude less than the levels in the primary zone. Finally, turbulent mixing and reacting flow complicate simulations with time scales of soot formation and oxidation substantially different from the time scales of heat release. Hence it is not surprising that authors are willing to present modeling results that agree only to within one to two orders of magnitude from the experimental values [Tolpadi, et al, 1997; Broklehurst, et al, 1997].

In the following paragraphs, a picture of soot formation in a premixed flame will be provided. In the subsequent sections, descriptions of each of the physical/chemical processes that must be treated in the modeling of soot formation in flames are briefly presented. The discussion will include gas-phase chemistry, particle inception, growth, agglomeration/coalescence, and oxidation. The importance of aerosol dynamics and its pressure dependence will be reviewed. In addition the application of such models to different flame types will be explored.

flame in fact creates the environment such that soot formation takes place in the post-flame region.

In the following several sections, brief discussions of soot inception, soot growth, soot oxidation, soot ageing, aerosol dynamics (free molecular, transition and continuum), and radiation.

Soot inception

The most ‘popular’ inception process utilizes the dimerization of pyrene [Appel, et al, 2000] to simulate the rate of soot inception. This methodology is closer to reality than the use of acetylene [Fairweather, et al, 1992] or naphthalene formation [Hall, et al, 1997]] that were utilized years ago. Still there is no evidence that such a sequence adequately describes inception. Also, the sensitivity of the total soot formation to the initial inception rates are, in many cases, weak as agglomeration/coalescence processes of many small droplets buffer any dependence on the inception process.

An alternate inception simulation of the inception process is utilized by Smooke, et al, [2005] who utilize a series of steady-state assumptions on intermediate species to estimate the formation of a large polycyclic aromatic structure. The model is based on the sequence of growing naphthalenyl to pyrenyl through sequential acetylene addition, H-atom elimination, H-atom abstraction, and acetylene addition followed by ring closure. Overall, the reaction can be written $C_{10}H_7 + 3C_2H_2 \rightleftharpoons C_{16}H_9 + 2H + H_2$. This sequence is assumed to continue to form yet larger PAH structures with the overall balance of $C_{10}H_7 + 3nC_2H_2 \rightleftharpoons C_{10+2n}H_{7+2n} + 2nH + nH_2$. Quasi steady-state concentrations of intermediate polycyclic aromatic hydrocarbons are assumed, leading to steady-state expressions for the formation rates of these high molecular weight condensed polycyclic aromatic hydrocarbons (PAH). In any solution methodology for modeling soot production, the source terms for conversion of gaseous species to soot must be accounted for by including the sink terms in the gas-phase equations. Here, ‘sink terms’ refer to the fact that gas-phase species can be consumed or formed during the formation or oxidation of soot particulates. In any fully coupled model, these sink terms must be added to the species conservation equations. Likewise, there is an enthalpy (sink) term that should be added to the gas-phase energy equation due to the formation of soot.

Surface Growth and Oxidation

A surface growth model used in numerical simulations is based on the premixed flame data of Harris-Weiner [1983] with an activation energy of $E_s = 31.8$ kcal/mole [Hura and Glassman, 1988]. Surface growth is first order in acetylene concentration in this model. Also available is the ‘MODFW’ surface growth mechanism [Colket and Hall, 1994]. This ‘CH’ model was shown to be successful in modeling soot growth in high temperature flames [Smooke, et al, 2000] and is similar to the HACA model [Frenklach and Wang, 1990]. Oxidation of soot by O_2 and OH is treated as described in [McEnally, et al 1998]. In the assumed free-molecule regime, surface growth and oxidation rates are proportional to the particle surface area.

Particle Dynamics

The growth of soot particles is modeled as a free-molecule aerosol dynamics problem, using the well-known sectional particle size representation for spheres. This method is preferred here as it provides much more detailed information on particle size distribution compared to the frequently used approach of the method of moments [Frenklach and Wang, 1990]. The application of the sectional approach to soot modeling is described in [Hall et al, 1997]. The contributions from the inception processes are incorporated as a source term in the dynamical equation for the first sectional bin, whose lower mass boundary is set equal to the mass of the assumed inception species. Calculated results were not significantly sensitive to the number of sections assumed, although 20 sections or more are preferred.

The spherical particle sectional model nominally imposes no constraint on the final particle size, and does not account for aggregate formation. Coalescence destroys particle surface area, whereas aggregation, to the first order, does not. This is an important consideration because of the dependence of surface growth and oxidation on particle surface area. Adding equations for the number of primary spheroids within a section make it possible to model accurately the formation of soot aggregates. Alternatively, an approximate treatment of the aggregate formation effects on surface area can be employed.

Soot Ageing

In practice, soot primary particles reach a maximum size due to active surface site deactivation (ageing). Dobbins [1996] has given a measured deactivation rate for the process, and some modeling of the effect has been carried out in premixed flames. Hall and Colket [1999] used a decay rate similar to that of Dobbins in a study of aggregate formation using sectional analysis, and Singh, et. al. [2005] tested different functional dependences of surface reactivity on age in their study of high pressure coagulation using Monte Carlo techniques. Appel, et al [2000] have fitted to various premixed flame data an empirical expression for the fraction of active sites that is a function of the average particle size and gas temperature, but not explicitly to individual particle age. Much remains uncertain about how to model this effect, particularly in a diffusion flame, however. Given this uncertainty, Smooke, et al [2005] have introduced a simple step function dependence of surface reactivity on particle size at which growth is shut off above a cut-off particle size (25 nm in their simulations). Modifications were also made to the coalescence model to account for aggregate formation.

2.2.3 Radiative Power Loss

For flames with sub-ppm soot volume fractions, the power radiated from soot and gas bands (CO₂, H₂O, and CO, using the exponential wideband model) is computed in the optically thin limit using the expressions developed by Hall [1994]. These flames will lose a very significant fraction of flame enthalpy due to radiation, and temperatures can be significantly depressed, affecting both flame chemistry and soot formation. In higher soot loading flames, the optically thin model tends to overestimate the radiation losses. In principle, some re-absorption of thermal emissions can occur, particularly on or near the

centerline of a coflow flame, which receives emissions from surrounding regions of the flame. This optical thickness effect reduces the net rate of thermal radiation energy loss and locally raises the temperature. Details of these calculations are provided by Smooke, et al [2005]. While temperature changes associated with radiation re-absorption are not large, the great sensitivity of soot growth to temperatures makes incorporation of these effects important.

3. Results and Discussions

3.1 Experimental Results

3.1.1 Selection of Additives

The initial focus of the work was to validate the methods and procedures by investigating the effect that ethanol has on reducing soot in ethylene flames. This chemical system was selected since substantial work has been performed on soot formation in ethylene flames, ethylene kinetics, and the use of ethanol for reducing soot. The baseline concentration of ethanol in ethylene was set such that the mass of oxygen in the fuel was 5% that of the carbon in the fuel. This same rule was utilized in other oxygen-containing mixtures. While this constraint puts the ‘additive’ concentrations very high, much greater than a few ppm, the team members had agreed that without the use of metal-containing additives, substantial reductions in soot would be difficult to achieve without large additive concentrations.

While these efforts were proceeding, AFRL was scanning a large number of (commercially-produced) fuel-additives in a gas turbine environment to help point the direction of subsequent work. More promising candidates included Brij-92, +100, a proprietary additive (referred here to PA), BHT and Kleen. Kleen is normally used in the racing car industry, and is composed of nitromethane, nitroethane, nitropropane, and cyclohexanone. The later phase of the project was focused on testing Kleen and its components. In addition, significant efforts were spent on investigating the use of pyridine. Motivation for its use is described in the following paragraphs.

An alternative proposal for suppressing soot production in gas turbine engines is accomplished by inserting a non-carbon species into the aromatic ring. Specifically, pyridine (C_5H_5N) is well known to have a low sooting tendency. Typically, it is argued that the cause of this low tendency is that with an N-atom in the ring, large pericondensed polyaromatic species cannot be formed, as the N-atom does not offer an additional unpaired electron for bonding external to the primary ring. This argument has been extended by suggesting that the lifetime of the intermediate radical (o-pyridyl) has a lifetime approximately 10,000 times shorter than the phenyl radical, a known intermediate species key to soot growth. In addition, 2-ringed species, e.g., quinoline (analogous to naphthalene in the pure hydrocarbon system), cannot not be formed readily due to (relatively) higher C-H bonding strengths at the meta position.

The ability of ring N-atoms to suppress soot growth/production in an otherwise hydrocarbon system has yet to be investigated. A variety of species could be used as precursor material. It is suggested to start with pyridine and if encouraging results are observed then alternate fuel additive compounds can be explored.

The concentration level of added nitrogen for the case of pyridine addition or for nitrate addition is a concern, as NO_x is also an important pollutant whose emissions are controlled. To estimate the level at which NO_x emissions might be a concern, typical

emission levels can be examined. The lowest NO_x emission levels for (large engine) commercial aircraft are above 30 NO_xEI or 30 grams NO_x (as NO₂)/kilograms of fuel. More typically, these emission levels are closer to 40-70, depending on the size class of the engine. Goals for future engines cruising at or near the ozone layer are closer to 10 NO_xEI. Hence, a level of nitrogen in the fuel that has the potential of producing an emissions index near 2 appears to be defensible. If a significant amount of the fuel nitrogen is fully reduced to N₂, rather than converted to NO_x emissions, then this constraint can be relaxed. Such phenomena is well-known in the literature based on studies of burning coal and synthesized liquid fuels from coal gasification/liquefaction or from shale oil.

A limit of 2 NO_xEI from the nitrogen in the fuel can be readily converted to a limit of 600 ppm of nitrogen in the fuel on a mass basis. This limit imposes a limit of 3400 ppm of pyridine (or its equivalent) in the fuel on a mass basis. Alternatively, in the case of nitropropane, an analogous argument suggests a slightly higher upper limit of 3700 ppm. As mentioned just above, in the case that some of this ‘fuel-bound’ nitrogen can be converted into molecular nitrogen, these low limits can be relaxed. There is a reasonable likelihood that these ‘upper limits’ maybe increased by a factor of 2-3.

These same arguments can readily be extended to the use of the nitro compounds, which also contain fuel-bound nitrogen; however, as the nitrogen atom is already bound with oxygen, it can be expected that the fraction of the nitrogen converted to NO_x emissions will be higher than would be the case for pyridine.

3.1.2 Flat Flame Burner Experiments

The team agreed that the first set of experiments would be performed on ethanol seeded ethylene flames as there was a reasonable amount of literature data on this chemical system. Hence these baseline experiments would help to validate the approach.

Results are reported for an ethylene/air flame with an equivalence ratio of 2.34. These results were obtained using the perforated plate, flame holder (Figure 1). The flame was also probed after the addition of ethanol which introduced 5% oxygen (by weight) into the fuel (with fuel defined as ethylene + ethanol) while keeping the total carbon flow constant. The experimental conditions are shown in Table 1.

Table 1. Experimental Test Conditions for the Premixed, Fuel Rich Flames

	Ethylene	Air	Ethanol
Flame	(slpm)	(slpm)	(ml/min)
1	1.38	8.41	0.00
2	1.25	8.41	0.335

The equivalence ratio of the base ethylene flame (Flame 1) is 2.34, selected for comparison to literature results. The flow rates for Flame 2 were set to provide the same carbon flow rate and an oxygen/carbon mass ratio in the fuel of 0.05. Temperature of the flame, measured as a function of height above the burner surface using an uncoated, type R, 0.003” butt-welded thermocouple, is shown in Fig. 18. At each height, the

temperature is determined using the TPD technique described in Liscinsky, et al (2000) whereby the thermocouple is rapidly inserted into the flame, using a pneumatically actuated sliding stage, while recording the temperature history of the bead. The bead response is corrected for radiation by balancing the heat transfer from the gas stream to the total radiation and then solving for gas temperature. Measured temperatures for both the ethylene and ethylene/ethanol flames are provided in Fig. 18. Also reported in the figure are the predicted temperatures using the SANDIA Premix code and the UTRC chemical reaction mechanism. The rapid fall-off in temperature in the post flame zone is under predicted by the code, despite inclusion of energy loss due to radiation from gaseous species.

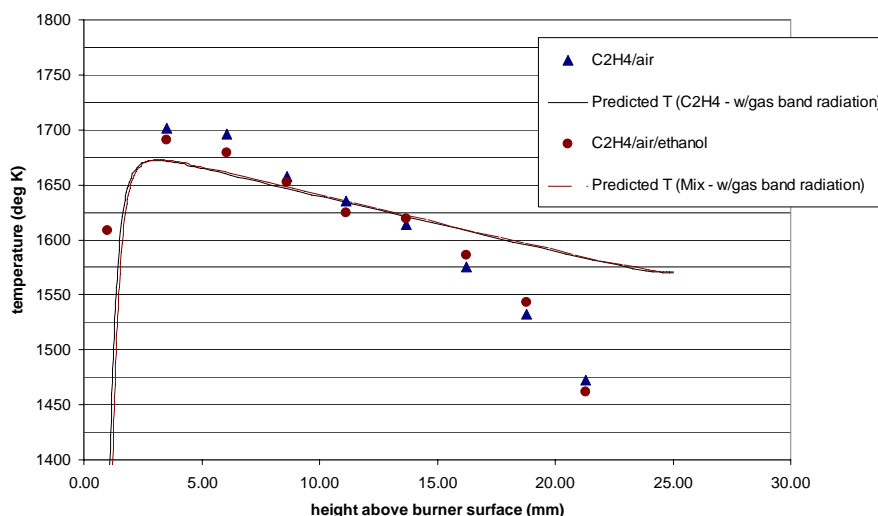


Figure 18. Temperature Along the Centerline of Flame 1 and 2

Soot volume fraction has been measured using Laser Extinction (LE) and Thermocouple Particle Densitometry (TPD). A full discussion of these diagnostics are reviewed in section 2.1 and can also be found in Liscinsky, et al (2000). Soot volume fraction as a function of height above the burner surface is shown in Fig. 19. Results are shown for Flame 1 using both LE and TPD as well as those from Xu et al. (1997) for a comparable flame with a carbon/oxygen ratio of 0.78. Despite the slight variation in experimental conditions for the Xu, et al work, the agreement between the three sets of measurements is very good. Soot volume fractions measured by TPD for Flame 2 are not in good agreement with the LE measurements, as there is nearly a factor of two between the two techniques. The TPD measurement depends not only on a curve fit to the temperature decay as the bead thermophoretically collects soot but also soot void fraction. Whereas measurements of soot void fraction for flame 1 have been made previously, measurements for flame 2 have not been collected and are recommended.

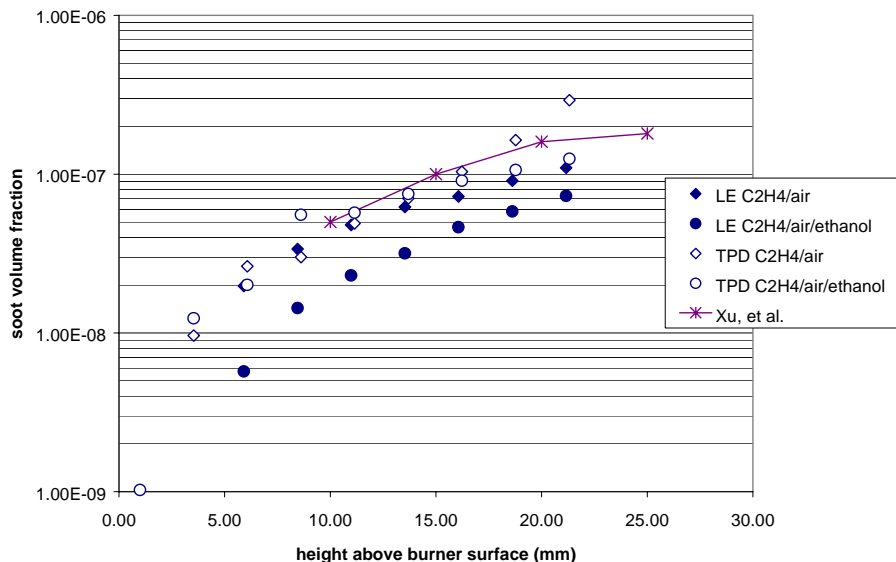


Figure 19. Soot Volume Fraction via Laser Extinction (LE) and Thermocouple Particle Densitometry (TPD) for Flame 1 and 2.

The laminar flame burner facility was modified to vaporize liquid fuels, premix with air and inject fuel-additives on line (see Section 2.1.2). Heptane, initially selected as the surrogate fuel for analysis was tested. Baseline studies indicated the existence of just a narrow operating region between the conditions at which sufficient soot was formed for reliable measurements and the flame lost its stability. Addition of 10% (by volume) of toluene slightly increased the soot production and increased the flame stability. A flame at equivalence ratio of 2.4 was selected as a reference condition. Soot volume fractions were measured for this base flame with peak soot volume fractions of approximately 0.2 ppm. The effects of a variety of additives were examined; including Kleen, ethanol, BHT, Brij-92, and the Betz JP-8+100 additive. For the latter three, there were uncertainties as it is unclear whether the fuel-additives were fully vaporized in the premixing/prevaporization zone. However, both ethanol and Kleen had measurable effects on reducing soot production at elevated additive levels (approximately 5%). Ethanol reduced soot levels by more than 70% and the commercial additive Kleen reduced soot production by about 20%.

Soot volume fractions as measured in the premixed 10% toluene/90% heptane flames with and without a variety of additives are shown in Figure 20. Additional results are summarized in Table 2 for each additive where the maximum fraction of soot reduced is indicated for a range of additive levels. This figure compares data from the reference, base flame without additives to results for several flames with additive concentration levels near 8000 ppm. In the case of ethanol, the additive concentration is set to create 5% oxygen in the fuel. These results clearly indicate that oxygenates, particularly ethanol and nitromethane, and pyridine have the largest impact on reducing soot production.

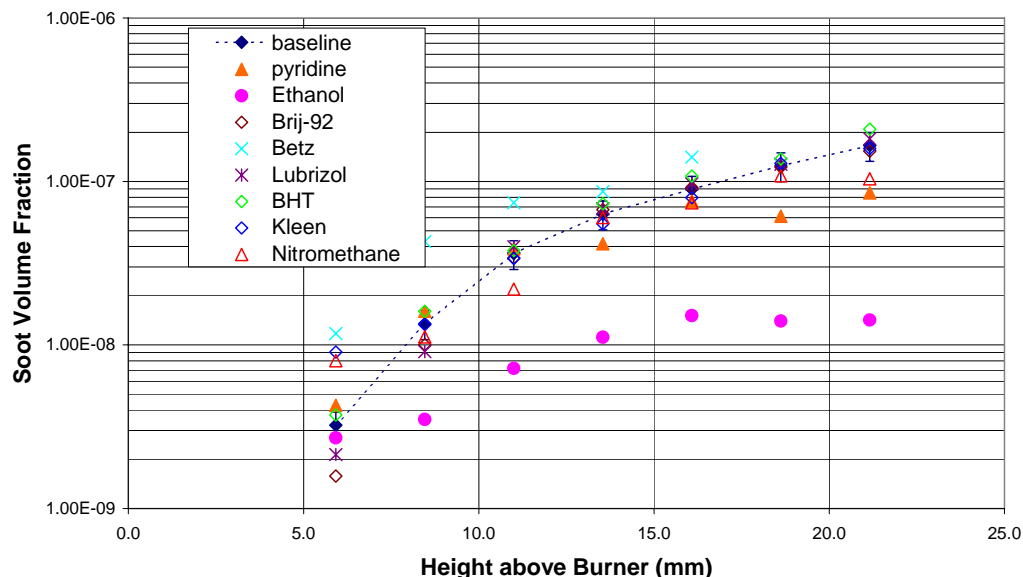


Figure 20. Soot Volume Fractions from Premixed, Laminar Flames. Base Flame is 10% Toluene and 90% Heptane.

Due to uncertainty in the measurements, changes less than 10% imply minimum impact by the additive. Pyridine was the most effective additive for reducing soot volume fraction in the premixed flame experiments. Data for this additive are provided in Figure 21, and demonstrate decreased soot formation with increasing additive levels.

Despite the very encouraging results with pyridine, soot samples extracted from the flame and analyzed by Scanning Electron Microscopy (SEM) indicate that primary particle diameter with pyridine added to the fuel are 10% higher than those produced in the baseline flame. The lower soot volume fraction, yet larger particle diameters, is consistent with the proposed mechanism by which pyridine reduces soot in the flames.

Meanwhile, particle diameters in samples from the flame seeded with Kleen are about 20% smaller those from the baseline flame.

Due to the expected dependence of surface oxidation rates on surface area, it is assumed that the lower soot volume fractions in the fuel-rich flames with added pyridine may not proportionally translate to the same fractional soot reductions from a combustor that includes soot oxidation. However soot emissions from combustors fed with Kleen may provide reductions greater than that suggested by Table 2.

Table 2. Percentage Reductions in Soot Volume Fractions in Fuel-Rich Premixed Heptane/Toluene Flames due to Presence of Various Fuel Additives.

Flame	Additive	Additive Concentration	Soot reduction
1	-	-	baseline
2	ethanol	5% O in C	~70 %
3	Kleen*	400, 800, 8000 ppm	<10%
4		24000, 48000 ppm	~20 %
5	Brij-92	400, 800, 8000 ppm	<10%
6	+100	400, 800, 8000 ppm	<10%
7	PA	400, 800, 8000 ppm	<10%
8	BHT	400, 800, 8000 ppm	<10%
9	Pyridine	5000, 10000, 50000, 100000 ppm	~30%
10		Nitromethane	5000, 10000, 50000, 100000 ppm

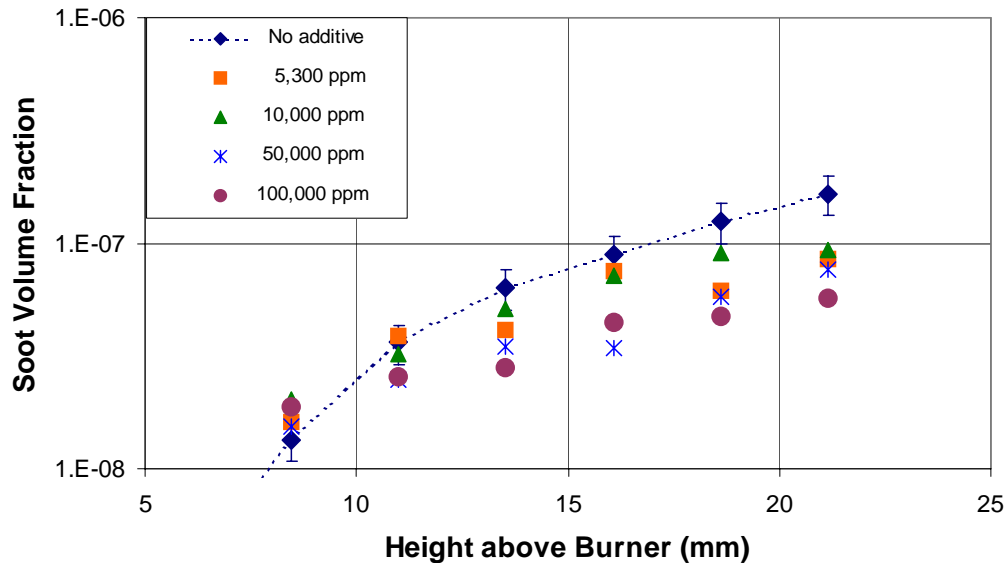


Figure 21. Reduction of Soot in Premixed Flame with Various Levels of Added Pyridine (as ppm in fuel)

In the work described above, the flame structure was not uniform as the flame front had a cellular structure. Initially, we believed the structure was a result of the geometry of the perforated plate (Fig. 1), which had been utilized to avoid condensation of the high molecular weight reactants (of interest in this work) within the cooled porous plug burner, which is conventionally used for flat flame burner studies. In an attempt to correct for this non-uniform flame front, we designed and constructed an uncooled porous plug burner made of hastalloy (see Fig. 4). We tested the new burner and found cellular flame structures nearly identical to those observed with the perforated plate. Hence, we

performed a literature review and were reminded of a well-known phenomenon for fuel-rich, premixed flames for fuels with high molecular weight (Strehlow, 1968). Apparently, this structure is due to large differential between thermal conductivity and species transport and/or differential species diffusion. The problem did not arise in the (previously-studied) ethylene flames, but became apparent for fuel-rich, premixed flames. The effect was aggravated by the increased molecular weight of the parent fuel. In this case, heptane and 20% toluene was the initial fuel. The cellular structure of the flame was mitigated by use of a porous plug burner and by addition of ethylene 25% by mass of the fuel.

The temperatures of the heptane/toluene burner-stabilized, premixed flames with and without pyridine were determined to assess whether the reduction in soot with added pyridine was due to a temperature shift. Several flames were investigated. Details of the flows are provided in Table 3, to facilitate modeling of these flames. As described previously, ethylene was added to avoid cellular flame structure with 25% ethylene and 75% primary fuel liquid on a mass basis. The primary fuel liquid comprises either 10% Toluene/90% heptane or 20% Toluene/80% heptane on a volumetric basis. Pyridine added 4% by mass of the fuel and the flow rates were 0.00820 grams/sec/cm².

Table 3. Mixture Mole Fractions and Fuel Mass Fractions for Premixed Flames.

Mixture Mole Fractions				
	10% Toluene	10% Toluene/ 4% Pyridine	20% Toluene	20% Toluene/ 4% Pyridine
C7H16	0.02846	0.02758	0.02481	0.02758
C7H8	0.00435	0.00421	0.00853	0.00421
C2H4	0.03864	0.03746	0.03888	0.03746
C5H5N	0.00000	0.00225	0.00000	0.00225
O2	0.19453	0.19452	0.19437	0.19452
N2	0.73402	0.73398	0.73341	0.73398

Fuel Mass Fractions				
	10% Toluene	10% Toluene/ 4% Pyridine	20% Toluene	20% Toluene/ 4% Pyridine
C7H16	0.657599	0.6309	0.569842	0.6309
C7H8	0.092401	0.08865	0.180158	0.08865
C2H4	0.25	0.23985	0.25	0.23985
C5H5N	0	0.0406	0	0.0406

The measured temperature profiles from thermocouple particle densitometry (TPD) are shown in Figure 22 and demonstrate that the pyridine additive does not affect the temperature profile significantly, although a slight increase of as much as 20K is possible high in the flame. (The baseline flames have no pyridine additives.) In contrast, the 10% toluene flame(s) have flame temperatures about 60K lower than the 20% toluene flames. Equilibrium (adiabatic) temperatures for these all of these flames are identical.

Soot measurements were also determined for the 10% toluene flames using laser extinction. They are shown in Fig. 23 with and without the pyridine additive. Pyridine reduces soot in this flame by about 20%, slightly less than that observed previously for a similar additive level. Modeling of these flames has been attempted, but is challenging due to the size of the mechanism and the requirement for the coupled transport and kinetics for the flame solutions. Note that recent suggestions (Krishnan, Lin and Faeth, 2001; Williams, et al, 2005) for the extinction coefficient of soot indicate that the actual levels of soot may be about 2 to 2 ½ lower than those reported in Figure 23, as we have used a earlier preferred value for this coefficient.

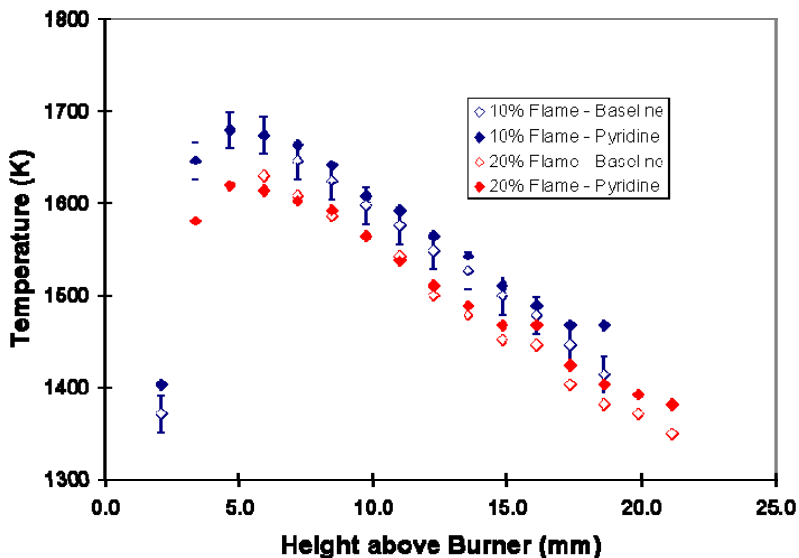


Figure 22. Measured Temperature Profiles for Several Premixed Flames.

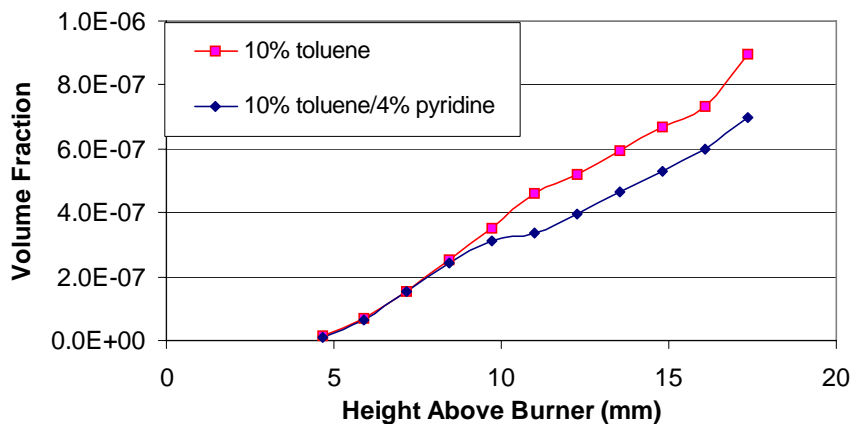


Figure 23. Comparison of Soot Volume Fractions (laser extinction) for Heptane/10% Toluene Flames.

A second experimental problem was associated with obtaining repeatable results with the new dilution probe (see Section 2.1.3 and Fig. 7). Careful control and monitoring of operating conditions are critical. In addition, the probe orifice through which the sample

is collected must be cleaned frequently. Furthermore, the clogging process is so severe, that medium and heavily sooting environments cannot be examined.

Additives studied have been performed using nitromethane, nitroethane, nitropropane and cyclohexanone, the primary components in Kleen which was found to have a relatively strong effect (see Table 4). Flame temperatures and soot volume fractions have been measured as a function of height above the burner surface. No discernable differences in flame temperatures were observed. At an additive loading of 4% by mass of oxygen, the most effective additives were nitromethane and nitroethane, with the former reducing the soot production by about 25% and the latter reducing soot production by more than 50%. For a flame with an equivalence ratio of 2.4, a comparison of the fractional reductions in soot as a function of additive levels is shown in Figure 24.

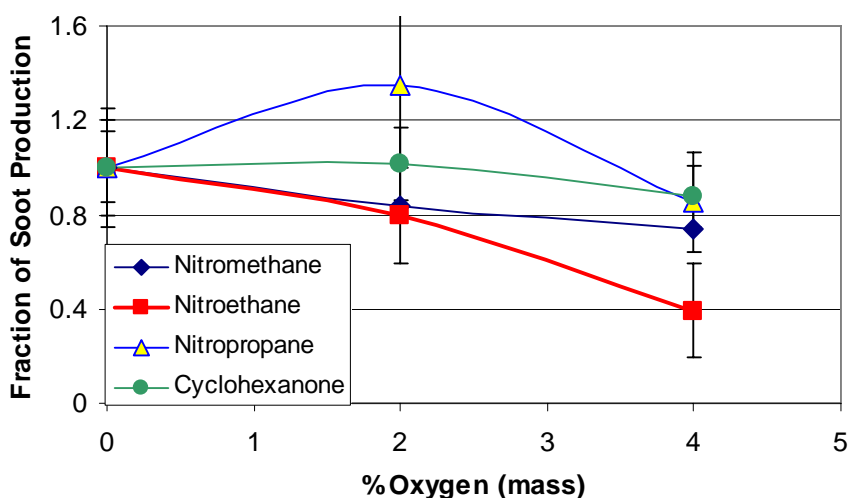


Figure 24. Relative Soot Production in Laminar Premixed Flame.

The most unusual feature of these data is the contrary effects of different levels of the additive, nitropropane. All of the results (and trends) have been confirmed by using a time tracing method. In these tests, the flame height was kept constant and the make-up of the inlet gases were altered in the following sequence: base flame, 4% oxygen (additive), base flame, 2% oxygen (additive). A typical time trace is shown in Fig. 25 for the nitropropane results which exhibited the unusual results of increasing soot at the lower concentration, but a soot reduction effect at higher concentrations.

Table 4. Particle Reduction Effectiveness of Kleen Components ($\phi = 2.4$)

Device		Nitromethane	Nitroethane	Nitropropane	Cyclohexanone
Premixed flame	4% Oxygen Heptane/toluene/ethylene	-25%	-60%	~15%	-12%
Premixed flame	2% Oxygen Heptane/toluene/ethylene	-15%	-20%	~30% increase!	-0%

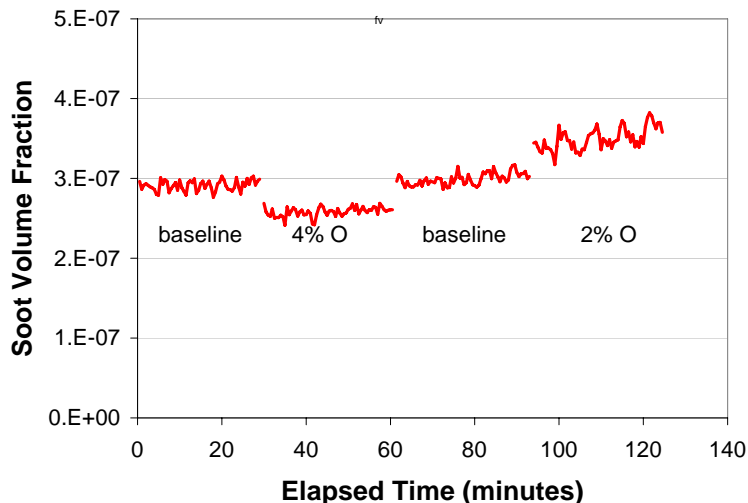


Figure 25. Time Trace Confirming Concentration Effect with Nitropropane.

Our interpretation of these results in the laminar, premixed flames is that a C_3 -hydrocarbon fragment (C_3H_5) from nitropropane enhances the propargyl radical (C_3H_3) concentration at low additive levels. Propargyl in turn is a known key intermediary to the formation of aromatic rings. We speculate that the formation of propargyl initially counterbalances any soot reducing potential that the nitrate group provides. But at higher additive levels, the C_3 level is saturated, and the effect of the NO_2 component dominates leading to reduced soot production. Nitromethane is a less active soot-reducing agent than is nitroethane since the former produces methyl radicals that add to C_2 hydrocarbons to form C_3 species. Nitroethane on the other hand is the most effective presumably because it barely perturbs the existing C_2 concentrations. Propargyl radicals are unaffected and there is no counterbalancing effect inhibiting the added NO_2 from reducing soot.

A schematic of the experimental set-up with the particulate sampling probe is provided in Section 2.1.4, Figure 9. This probes enables rapid high dilution rates ranging from several hundred to a hundred thousand. In this manner, the sample can be rapidly ‘frozen’, transported to the analyzer and particle coagulation and wall loss can be minimized.

Figure 26 depicts the problem with probe clogging in which particulate-laden samples are extracted from the flame and sent to a scanning mobility particle sizer (SMPS) and then to a condensation nuclei counter (CNC). Once the experiment is set-up, an initial sample stream is collected (R28) and then after a few moments, a second sample (R29) is obtained. Significant degradation in the total particle count and in the particle distribution is observed. However, upon cleaning the probe orifice (mechanical insertion of a fine thermocouple wire into a 0.007” hole) and collecting another sample (R31), then the original count and distribution is recovered.

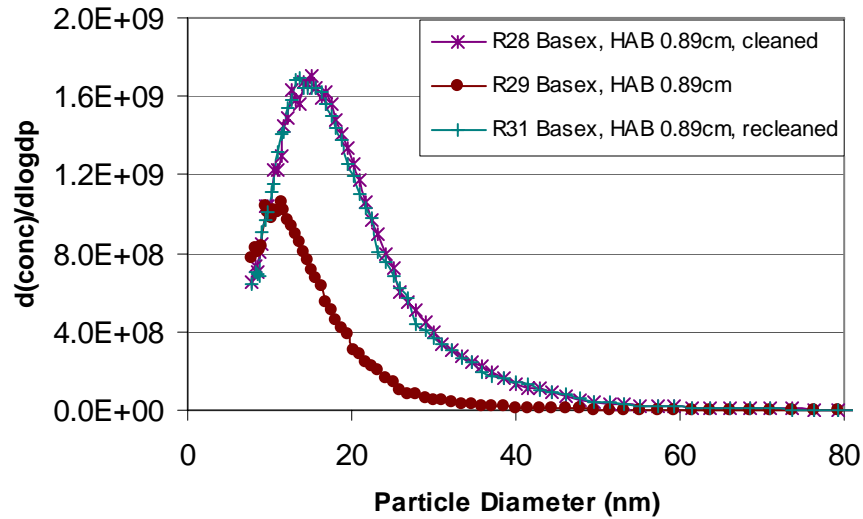


Figure 26. Degradation of Diluted Sample (raw signal) due to Orifice Clogging.

Raw (i.e., highly diluted) samples of particle size distributions as a function of height above the burner are shown in Figure 27. As can be observed, there is a dramatic shift in the size distribution within only 2.5 mm within the flame. Absolute values of this distribution have not yet been determined, although the relative distributions should be valid.

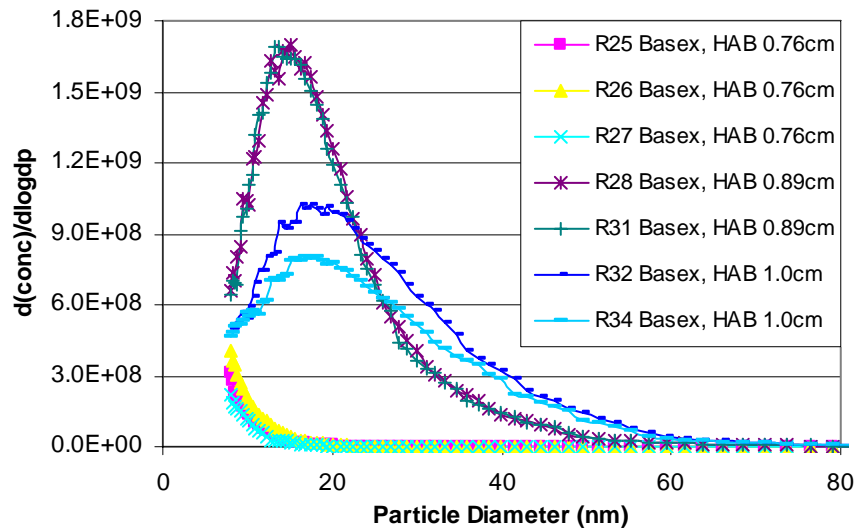


Figure 27. Particle Size Distributions in Diluted Samples.

Particle Size Measurements in Premixed Flames

The effectiveness of nitromethane, nitroethane, nitropropane and cyclohexanone in premixed laminar heptane/toluene/ethylene flames was reported previously using laser extinction to measure soot volume fraction. To further investigate those results, thermophoretic sampling was combined with scanning electron microscopy to measure particle size. A brief description of the sampling technique is provided in Section 2.1.3.

The TEM grids onto which particles were collected via thermophoretic sampling were analyzed by scanning transmission electron microscopy (STEM) at a magnification of 40,000. Samples obtained at a height of 12.3 mm above the burner surface were compared for 3 different additives (nitromethane, nitroethane and nitropropane). The additive concentrations were set so that oxygen addition was 4%. The photomicrographs are compared in Figure 28 with the particle size statistics shown in the adjacent table. The results show that the nitroethane produced the smallest size particles. This observation is consistent with the laser extinction measurements indicating that nitroethane was the most effective additive in the premixed, flat flame studies.

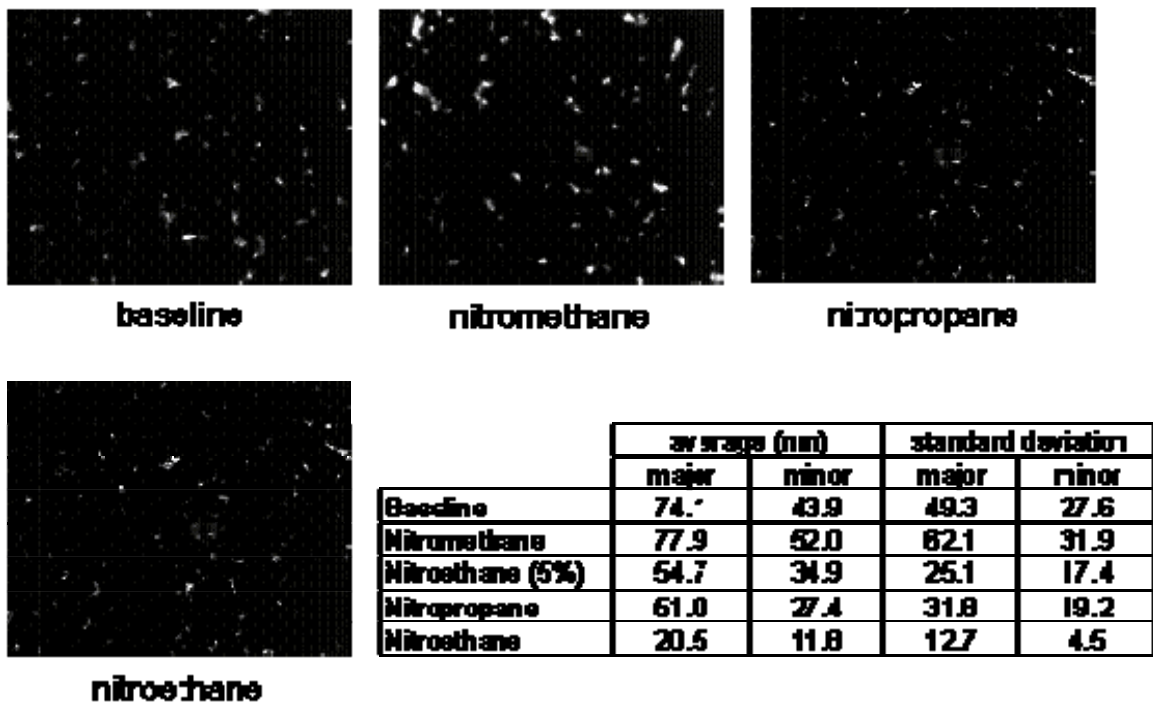


Figure 28. Photomicrographs of Particulates Collected from Premixed Flames using Thermophoretic Sampling.

3.1.3 Combustors

Fuel-Additive Tests in Combustor

In experiments, piggybacked onto a Pratt and Whitney combustor development program, attempts were made to measure particulate with and without the additives +100 and pyridine. Diagnostics included a new tapered element oscillating mass meter and the scanning mobility particle sizer. A new probe was utilized and nitrogen dilution was added to the sample probe at the probe tip. By variation in the dilution flow rates, dilution rates above 10 were achieved. Particle size distribution and mean particle size were shown to be affected by the dilution rates. The highest dilution levels appear to freeze the particle size distribution. The additive injection system failed during initial tests and tests were repeated.

The fuel additive tests were conducted in a prototype aeroengine burner at moderate temperature and pressure conditions during a sector test of an advanced commercial PW combustor. Data were acquired at 2 different combustor conditions with 2 different additives as shown in Table 5. The combustor was operated on Jet A. The two additives were the +100 additive package and pyridine. For reference, the recommended amount to form JP8+100 is 256 ppm of the +100 additive package. Using high-pressure syringe pumps, additization was performed to achieve the additive concentrations shown in Table 5. The additives were injected into the main Jet A fuel supply well upstream of the fuel nozzles in order to ensure thorough mixing. Additization was performed for 3 min before data was acquired and the concentration changes were made sequentially.

Table 5. Test Conditions for Combustor Sector Testing

Pressure (psia)	Temperature (deg F)	fuel /air Ratio	+100 (ppm)	Pyridine (ppm)
240	900	0.030	256	0
240	900	0.030	500	0
240	900	0.030	1000	0
240	900	0.030	2000	0
240	900	0.030	4000	0
240	900	0.030	0	256
240	900	0.030	0	500
240	900	0.030	0	1000
240	900	0.030	0	2000
240	900	0.030	0	4000
240	900	0.030	0	8000
65	420	0.024	256	0
65	420	0.024	2000	0
65	420	0.024	0	256
65	420	0.024	0	2000

Particle samples were acquired using the sampling system shown in Fig. 15 with a water-cooled dilution probe specially suited for particulate sampling. Sample dilution at the probe tip can be shown to (help) preserve particle size distribution. The internal geometry of the probe tip is shown in Fig. 16. The probe was located at the midpoint of the combustor sector and was stationary during testing. For the reported results the probe was operated with an 11:1 dilution ratio, which was found in separate tests to essentially freeze the particle size distribution for similar conditions.

Particle size distributions were acquired using a TSI Scanning Mobility Particle Sizer to determine particle size and number density from 10 to 385 nm. A typical size distribution is shown in Fig 29. Measurements of the particle emissions for each of the additives are shown in Figs. 30-33. Little effect of dilution ratio on median particle diameter or particle number density is observed as a function of additive concentration.

However the effect of combustor condition is observed by a decrease in median diameter and number count for the combustor temperature, pressure and f/a.

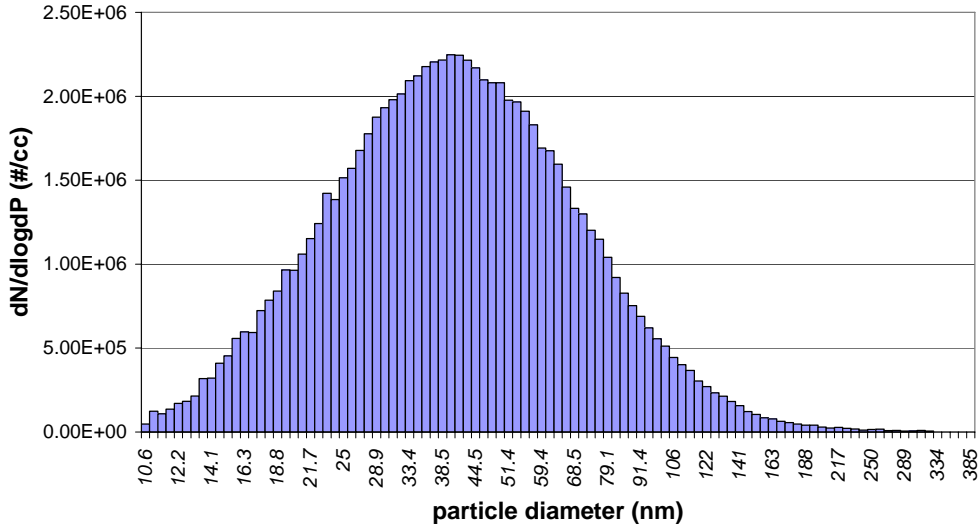


Figure 29. Typical Particle Size Distribution in Combustor Experiments.

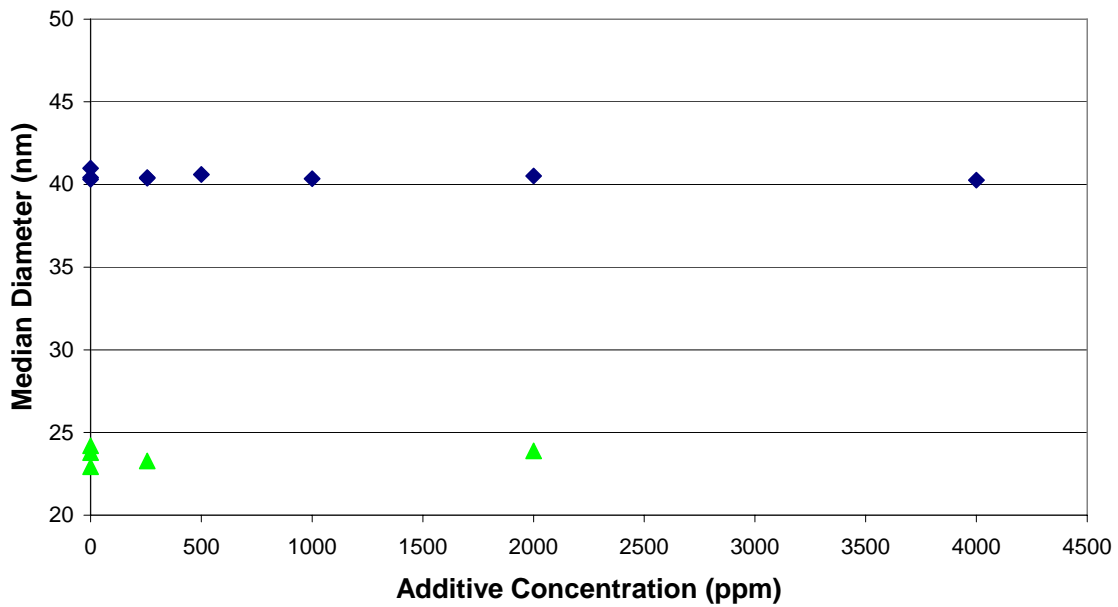


Figure 30. Effect of +100 on Median Particle Diameter (diamonds = 240 psia, 900 deg F, triangles = 65 psia, 420 deg F).

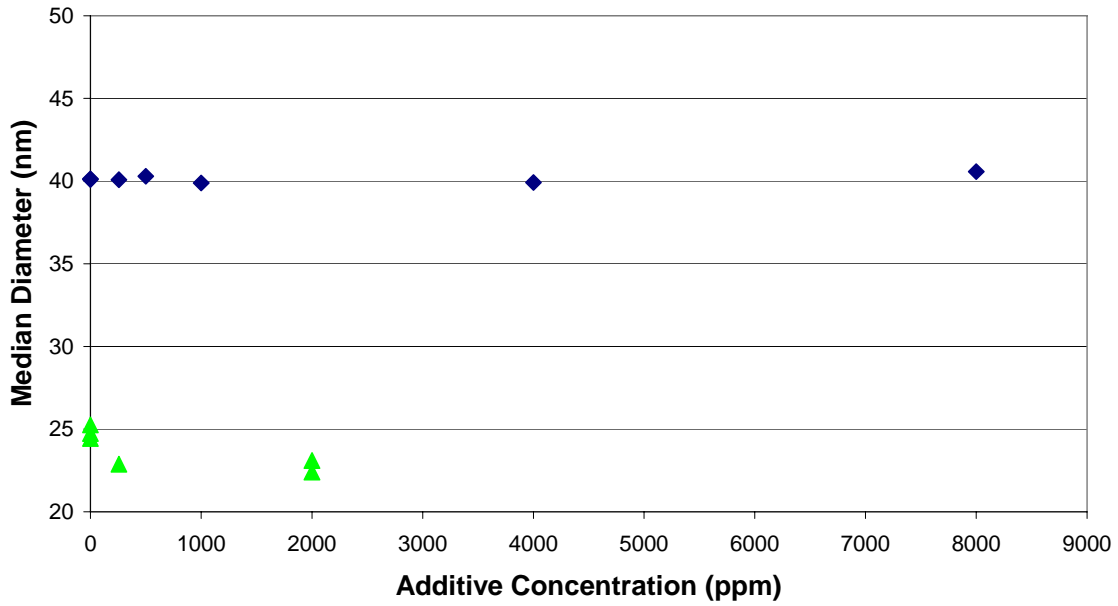


Figure 31. Effect of Pyridine on Median Particle Diameter (diamonds = 240 psia, 900 deg F, triangles = 65 psia, 420 deg F).

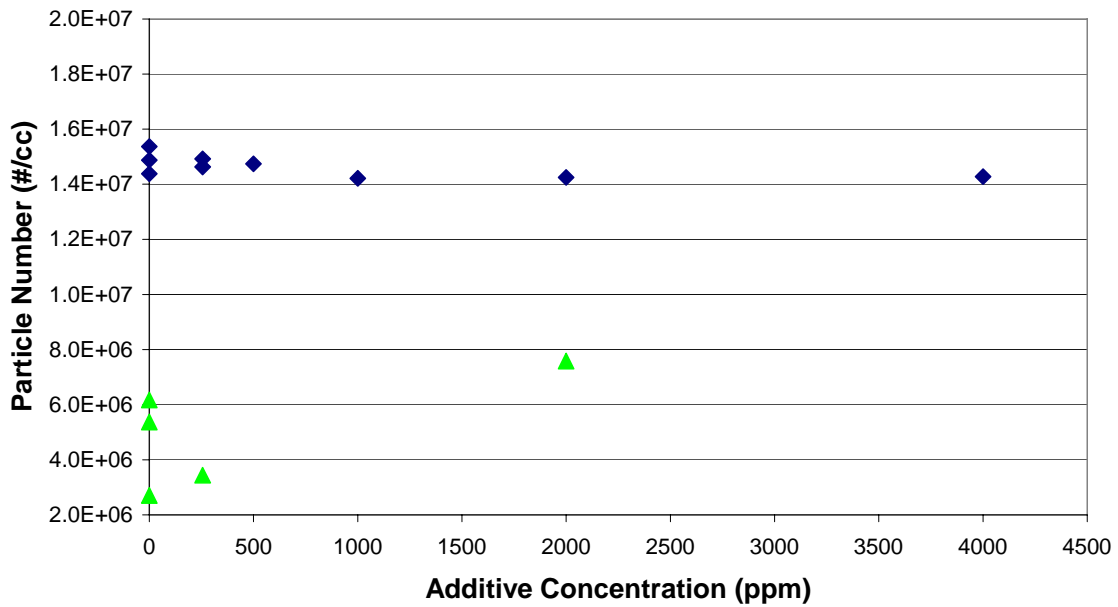


Figure 32. Effect of +100 on Particle Number (diamonds = 240 psia, 900 deg F, triangles = 65 psia, 420 deg F).

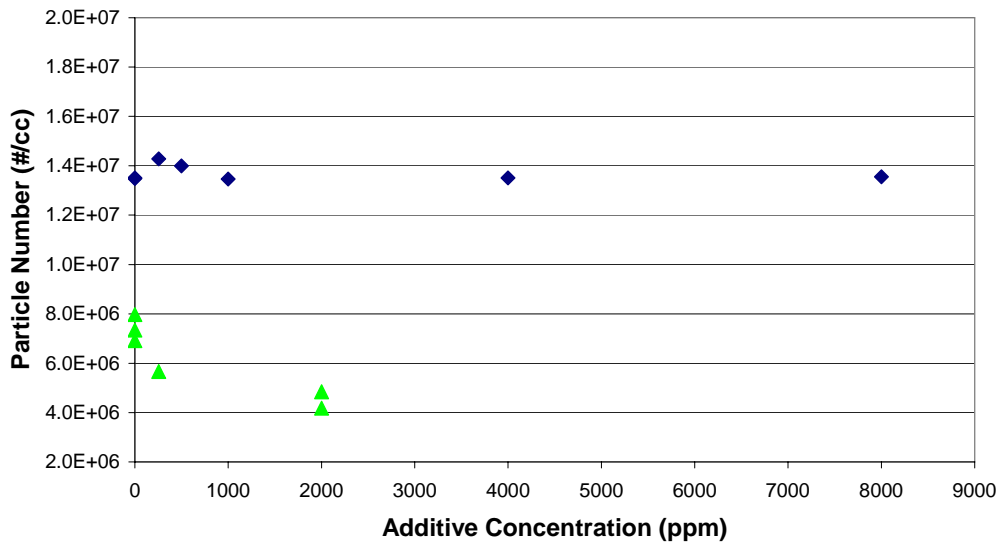


Figure 33. Effect of Pyridine on Particle Number (diamonds = 240 psia, 900 deg F, triangles = 65 psia, 420 deg F).

Loss of particulates in sample lines

Quantitative sampling of particles and the particle size distribution remains an issue as shown in our previous studies when comparing experimental data and calculated particle size distributions and total mass. An excel-based, particle line loss model has been developed based upon work performed by Yook and Pui [2005] under a NASA funded contract. The model includes losses due to thermophoresis, diffusion, inertial impact and electrostatics. These processes are all first order in particle concentration and hence are independent of number density. It is assumed the sample stream is sufficiently diluted such that particle coalescence can be neglected.

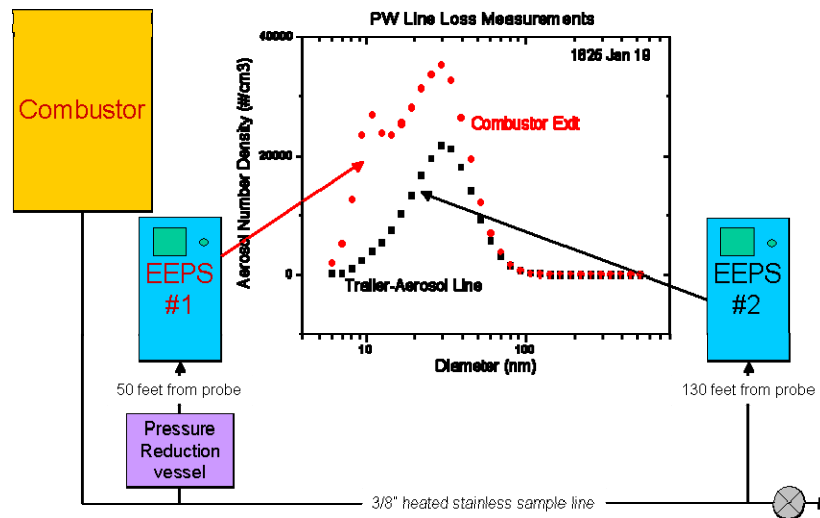


Figure 34. Schematic of Hardware and Results for Particle Line Loss Determinations.

Under PW and NASA funding, line loss measurements have been made in the PW Middletown X960 test stand with a full annular combustor with participation from NASA Langley. This facility includes a new independent sampling system to extract particulate measurements; it includes a sampling rake of three (tip dilution) probes. Size distributions were determined at two locations along the sampling line using two identical instruments: TSI 3000 Engine Exhaust Particle Sizer (EEPS). This instrument recorded a particle size distribution consisting of 32 channels from 6.5 to 532 nm at 10 Hz, one owned by UTRC and the second owned and operated by NASA Langley (courtesy of Bruce Anderson). A schematic of the sampling line with instruments is shown in Figure 34, along with the size distributions measured at the two locations.

The first peak in the red points at 10-12 nm are believed to be due to condensation phenomena occurring within the pressure reduction vessel and should be ignored. The substantially elevated particle count at low particle size as observed by the first instrument is however believed to be real and is due to sampling line losses.

The line loss model was utilized to compare with these data. Figure 35 shows a comparison of these data (when converted to penetration efficiencies) and the predictions from the model. (Note that the condensation peak has been ignored.) Comparison is very good, except for the high particle sizes (greater than 100 nm) for which the uncertainty in measured particle count is high. An analysis of the loss mechanisms indicates that for the small particles, diffusional effects dominate the losses. An analysis is underway to recommend ideal sampling conditions to minimize line losses.

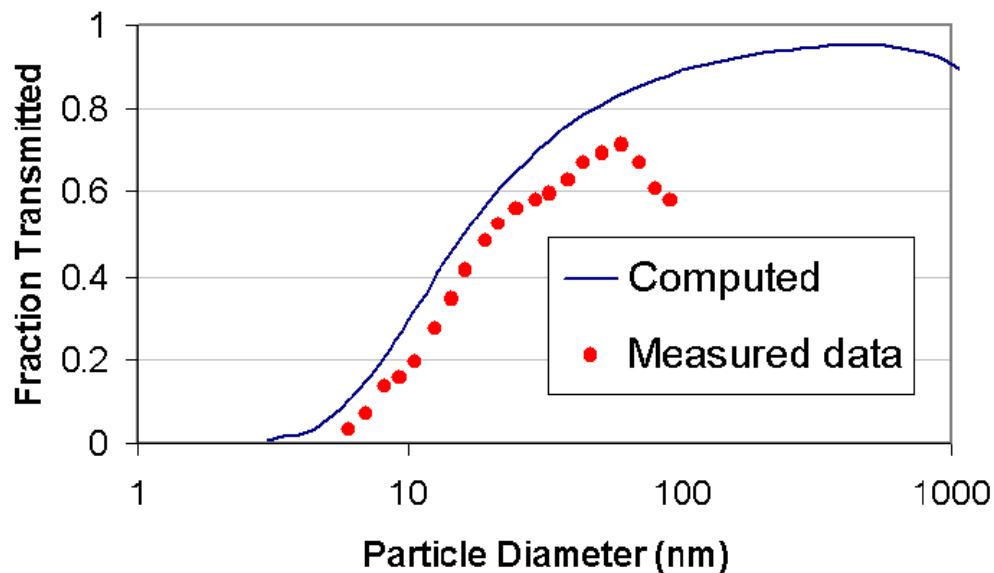


Figure 35. Penetration Efficiencies of Particulates

3.2 Soot Modeling

3.2.1 Gas-Phase Kinetics and PAH Chemistry

The mechanism reduction process was a relatively straightforward effort, consisting of elimination of reactions and species larger than pyrene ($C_{16}H_{10}$). The reduction was motivated by the added computational expense associated with the original mechanism that included species ($C_{30}H_{14}$) and reaction mechanisms that were nearly twice as large as pyrene. The reduction process was justified by the increased uncertainty of the thermodynamics, the reaction processes, and their rates with increasing molecular size with little added benefit to assessing the relative effectiveness of a soot-reducing additive. The net result was a reduction in the number of species by 20% (367 to 283) and the elimination of the number of associated elementary reactions (1850 to 1647). Furthermore, in most soot formation models, soot inception is based upon species (or their formation rates) that are equivalent to or smaller than the molecular weight of pyrene.

Pyridine (C_5H_5N), which has a nitrogen atom embedded into the aromatic ring, had been identified in previous work at UTRC to reduce soot from fuel-rich premixed flames. Levels as high as 100,000 ppm pyridine (in a heptane/toluene fuel blend) were used to achieve as much as 40% reduction in the soot produced from a premixed flame. Results obtained at other team-member laboratories have been mixed, although soot reductions had been observed at one other organization (PSU) in a turbulent flame. Based on these results, an effort was initiated to develop a modeling capability for examining effects from pyridine. A sub-mechanism was assembled based upon the pyrolytic studies of Mackie, et al (1990) and subsequent work on the oxidation of pyridine Ikeda, et al (2000). This sub-mechanism was added to the heptane reaction set and several additional steps were added to include trapping of C2-hydrocarbons by fragments of the pyridine molecule. The revised, total reaction set consisted of 314 species and 1713 reactions.

Two kinetic mechanisms were used in this study. The first was the detailed reaction set provided by M. Frenklach (ref) and modified at PSU to include oxygenated compounds. It includes species as large as pyrene (a four ring polycyclic aromatic hydrocarbon, $C_{16}H_{10}$, with a mass of 202 atomic mass units, or amu). In addition, the PSR model was run with another detailed reaction set for ethylene that has been utilized in previous soot modeling efforts (Colket and Hall, 1994 and Hall, et al, 1997) in laminar premixed and diffusion flames. To this mechanism, species, reactions and related thermodynamics for the ethanol chemistry originally developed by C. Westbrook (Lawrence Livermore Laboratories), and as extracted by T. Litzinger (at PSU) have been added. This latter mechanism will be referred to as the UTRC mechanism.

3.2.2 Soot Modeling – Flat Flame

Predictions using the revised kinetic set were performed to assess the effect of pyridine on modifying the gas-phase chemistry and the precursors to soot. Initially, isothermal conditions at one atmosphere were assumed just to assess the reaction chemistry. The equivalence ratio of the mixture was assumed to be two. Computations were performed at

1400K and 1600K with no pyridine added and with 1% pyridine added to the fuel – heptane. In addition, a separate set of computations was performed without the reactions speculated to inhibit aromatic growth. Computed values of naphthalene are shown in Fig. 36, and indicate only a small decrease (~5%) in the naphthalene concentration with 1% pyridine added. The decrease in pyrene was as much as 10% through addition of pyridine.

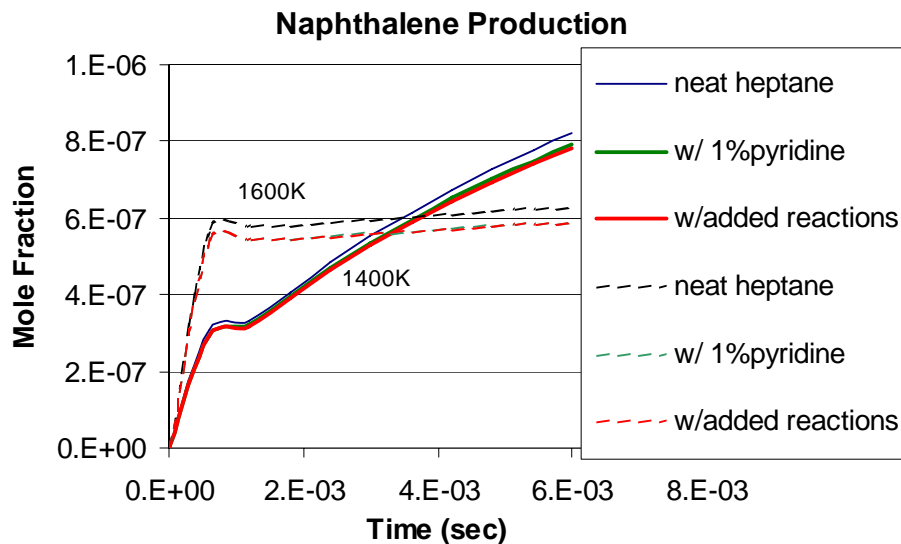


Figure 36. Comparison of Predicted Naphthalene With and Without Added Pyridine.

Recently, the complete chemical kinetic mechanism has been utilized to predict chemical kinetic effects occurring within a premixed flame when pyridine is added. Two flames were studied. The first is a heptane/toluene/ethylene fuel rich flame. As discovered earlier in the project, fuel rich flames with high molecular weight fuels (such as heptane and/or toluene) are subject to cellular formation due to differential diffusion between the oxidizer and fuel. Ethylene mitigates the effect. For the second flame, about 3% of the fuel was replaced with added pyridine. The overall equivalence ratio for the two flames was 2.39. Computations were performed with Sandia's CHEMKIN Premix code using flow rates matched to experimental conditions and using a previously measured temperature profile (same assumed for both flames). Obtaining converged solutions was challenging, but eventually we modified an approach developed by colleagues (Litzinger) at PSU (working on the same SERDP project) to get converged flame solutions. Comparisons of profiles of benzene, naphthalene, phenanthrene, and pyrene for the non-seeded and the pyridine-seeded flames are shown in Figure 37.

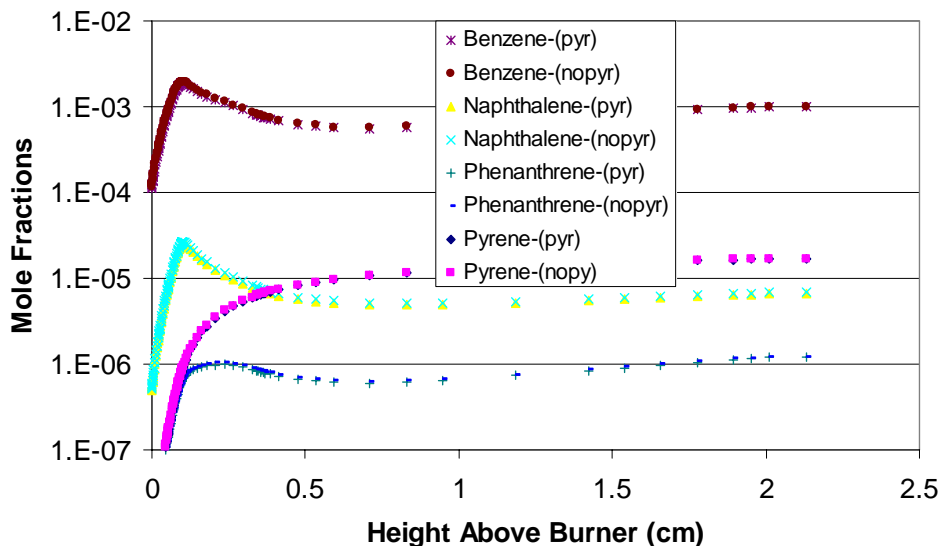


Figure 37. Comparison Of Computed Mole Fractions For Several Species As A Function Of Height Above The Burner For Fuel-Rich, Premixed Flames With And Without Added Pyridine.

Clearly the differences are virtually negligible. To accentuate the differences, the mole fractions from the pyridine-seeded flame were normalized by those from the non-seeded flame. The results are plotted in Fig. 38.

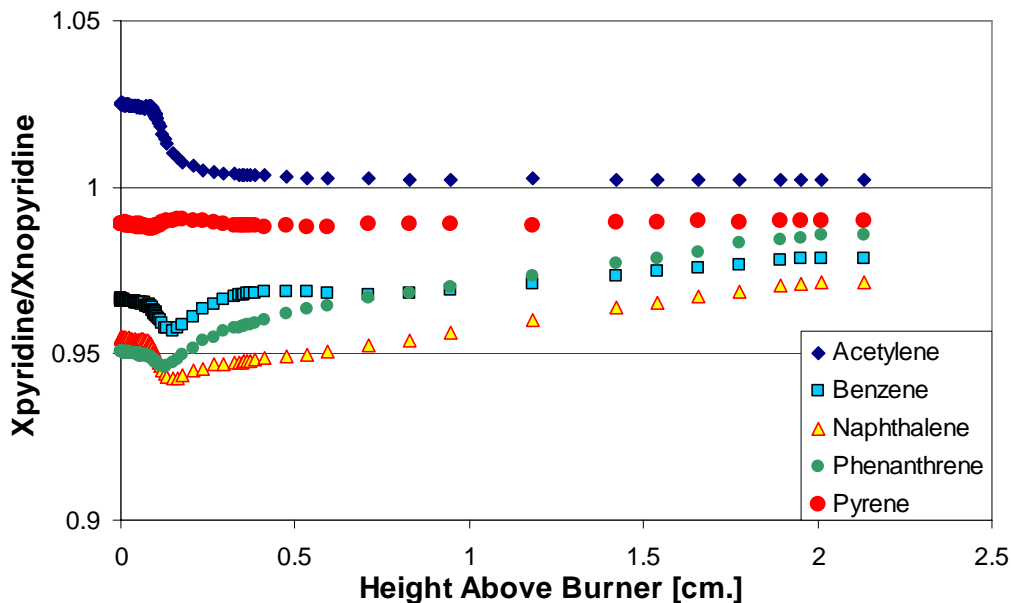


Figure 38. Normalized Concentrations Of Key Species In Fuel-Rich Premixed Flames With Added Pyridine.

The odd shapes low in the flame (~ 0.15 cm) can be ignored as this is the preheat portion of the flame and little chemistry is occurring. The early values of the normalized benzene concentration are about 3% lower than the 'neat' values (those with no pyridine added). This reduction is directly in line with the fact that the initial value of toluene (the primary source of benzene) is diluted by 3%. The initial concentration of naphthalene is reduced

by more than 5%, consistent with arguments that have been previously proposed for why pyridine should suppress soot production. However, the relative suppression of phenanthrene formation is not as great, and the pyrene concentrations are affected by only 1%. Hence the predictions leave open some questions and uncertainties regarding the effectiveness of pyridine as soot-reducing agent. Note that while the trend observed in the modeling was the same as observed in limited experiments, the level of decrease was sufficiently small that further modeling work in this area is not warranted without additional experimental confirmation of the effectiveness of this molecule.

3.2.3 Soot Modeling – Well Stirred Reactor

Reactor Simulations

Simulations of the toroidal Well Stirred Reactor (WSR) experiments at WPAFB (Stouffer, et al, 2002) have been performed using a modified version of the Perfectly Stirred Reactor (PSR) code (Glarborg, et al, 1986). The modified code has the soot equations fully coupled into the solution algorithms. In addition, a version of this ‘sooting’ PSR code is available that also can be run with an arbitrary network of individual PSRs. Both the PSR and network PSR code have the soot sectional equations (Hall, et al, 1997) fully imbedded, treating inception, growth, particle dynamics, and oxidation. Scrubbing of the gas phase species due to their conversion to soot particles and gaseous species formed or altered during soot oxidation is included in this model. The reactors can be assembled for a streamline analysis or can be used in a network with any arbitrary sequence of reactors in series or parallel.

Normally, only exit gas-phase species concentrations and temperatures are determined by the PSR code. The modified code also computes the particle size distribution, from which total particle mass and number densities can be calculated. Details are provided in Colket, et al, (2004). In addition, a correlation developed at UTRC for the relationship between smoke number and total particle mass concentration (mg/m^3) where the volume is based upon conversion of the flame gases to atmospheric pressure and at 289 K. Ambient conditions are utilized for the reactor studies as they are close to characteristic conditions for the smoke number measurement device.

Simulations of the jet-stirred reactor studies were performed with this ‘sooting’ PSR code. Reactor volume and mass flow rates were matched to the experimental conditions for cases with pure ethylene as the fuel as well as for the ethylene/ethanol blend. Adiabatic conditions were assumed. For the UTRC reaction set, predicted Smoke Numbers are shown in Fig. 38. Comparisons to experimental data sets indicate that the UTRC model under predicts slightly the level of smoke produced in the experiment, although the trend is well matched (see Colket, et al, 2004). The UTRC model predicts a slight increase in Smoke Number when ethanol is added, consistent with a slight increase in soot mass. The experimental results exhibit a similar trend for the two fuels. The Frenklach model indicated soot is reduced with added ethanol.

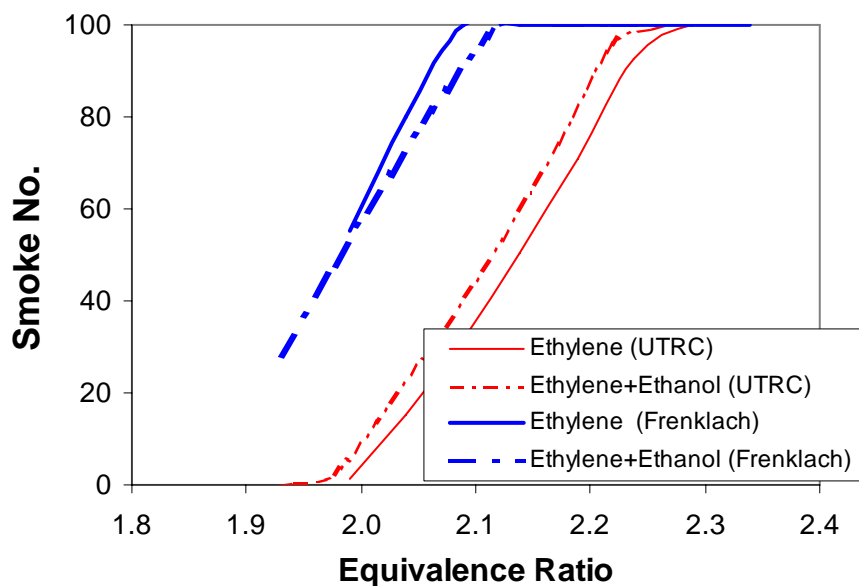


Figure 39. Predicted Smoke Numbers in PSR Using Two Kinetic Mechanisms for Ethylene and Ethylene with Ethanol Additive

As shown in Figure 40, the computed temperatures are about 40K lower for the cases with the additized fuel. Soot formation is known to be a strong function of temperature (Glassman, 1989), the difference in temperature likely contributes to the different soot levels. The dependence of soot formation on temperature depends on which side of the ‘bell-shaped’ curve the experiments have been performed. The negative trend (decreasing soot with increasing temperature) suggested the tests have been performed on the high temperature side of the soot bell.

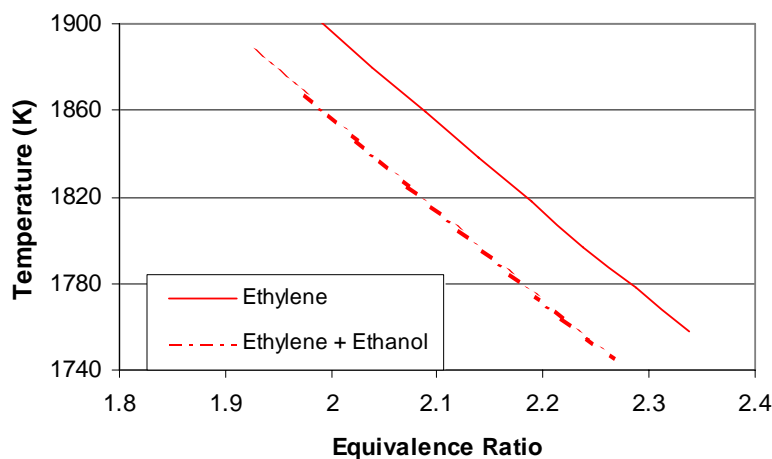


Figure 40. Predicted Temperatures in PSR for Ethylene and Ethylene with Ethanol Additive using the UTRC Kinetic Mechanism.

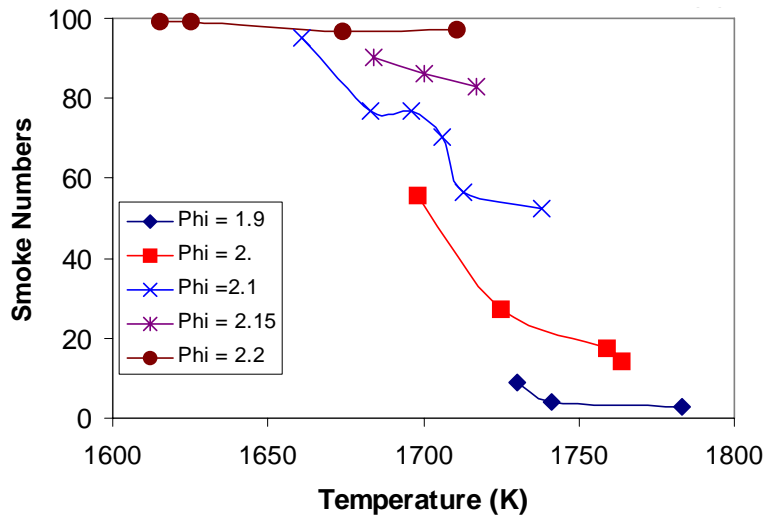


Figure 41. Measured Smoke Number as a Function of the Experimental Temperature.

A detailed analysis of the experiment indicates that this prediction was correct. A plot of the measured soot levels as a function of the reaction temperature is shown in Fig. 41, where the data was obtained from S. Stouffer. The data clearly show how the temperature and soot are inversely related (either for different equivalence ratios, or for constant equivalence ratios); hence the data was indeed obtained on the high temperature side of the bell curve and the results in Fig. 41 are therefore explained (given the temperature differences provided in Fig. 36). (The data for constant equivalence ratio and different temperatures were obtained during very slow transients after the reactor flows were readjusted to a new set of conditions, and before the reactor temperature had stabilized.)

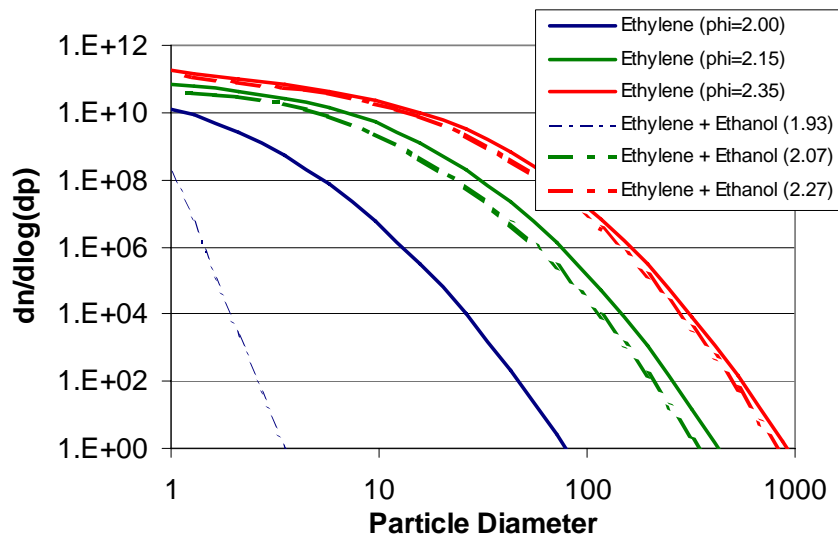


Figure 42. Predicted Particle Size Distributions (nm) for PSR using UTRC Mechanism.

Additional information on the computed solutions is provided in Fig. 42 in which the size distribution of soot particles is provided for a range of equivalence ratios with and without the presence of the ethanol additive. The number densities keep increasing with

decreasing particle size. These results are unusual with respect to typical profiles for combustors in which a clear maximum in the particle size distribution usually occurs (Liscinsky, et al, 2001). The predicted results for this stirred reactor study needs experimental confirmation.

Simulations were also performed using the Frenklach mechanism. Use of this detailed reaction set resulted in larger predictions of aromatics (typically more than a factor of 10) than those levels predicted from the UTRC mechanism and hence heavier soot loadings are also predicted. Trends with the Frenklach mechanism are similar to those described for the UTRC mechanism.

Some analysis of the well-stirred reactor studies has continued. An issue of concern has been the understanding of the apparent increase in the soot production with the fuel-additive ethanol. Ethanol when added to ethylene fuel in the well-stirred reactor (WSR) experiments had the opposite effect on smoke number as did the premixed flame experiments. The stirred reactor environment is noticeably different from the premixed flame as the products are intermixed with the unburned reactants. Using correlations of smoke number, increases in particulate mass emissions with added ethanol were on the order 20-40% for a given equivalence ratio. This contrasting effect has been traced principally to a temperature effect. In the case of the premixed flames, the computed flame temperatures increased by only about 5 K and the experimental temperatures increased by about 15 K, differences that are less than the uncertainty of the measurement. In contrast, for the WSR and for constant equivalence ratio conditions, temperatures decreased by about 40-50 K for both the experiments and for the modeling results. Temperature is well-known to be a key parameter in the formation of soot. Both experiments and modeling of soot formation in the WSR at a constant equivalence ratio (ethylene only) demonstrated that the conditions in the WSR are on the high temperature side of the bell. (The existence of a soot bell in which soot formation rates first increase with increasing temperature, but then decrease with further increases in temperature is well-established.) Hence, decreases in temperature increase soot production. These effects are explained further in the following paragraphs.

At low temperatures when temperature and soot production follow parallel trends, the soot production is kinetically limited. But on the high temperature side of the soot bell, characteristic of our WSR, the thermal stability of aromatic species falls off with increasing temperature. Benzene and other aromatics are recognized to provide the foundation for soot formation (inception) and growth. Loss of these species directly inhibits the production of soot. Specifically, the thermal decomposition of a key intermediate species (e.g., phenyl radical or C_6H_5) through $C_6H_5 \Rightarrow 1-C_6H_5 \Rightarrow C_4H_3 + C_2H_2$ increases rapidly with increasing temperature and becomes first competitive with and then dominates over growth reactions (e.g., as initiated by $C_6H_5 + C_2H_2 \Rightarrow C_8H_7$).

This effort has demonstrated that in the case of the WSR, in which the reactants (e.g., molecular oxygen) are also present in the soot formation zone, low activation energy oxidation step(s), such as



shift the soot bell to much lower temperatures than are normally observed in flames. Stirred reactors are often utilized to simulate combustor environments, and the (changing) shape of the soot bell may be an important concern as we apply our work to gas turbine engines.

Contrasting experimental trends observed in the well-stirred reactor experiments at WPAFB (Stouffer, et al, 2002; Reich, et al, 2003) have been examined and explained by utilizing a modified version of the CHEMKIN II-based code for stirred reactors (Kee, et al, 1991; Glarborg, et al, 1986). The code has been modified to include conservation equations for soot aerosols with treatment of particle inception, particle growth, aerosol dynamics, and particle oxidation. These equations are fully coupled to the gas-phase species by including terms to account for scrubbing of the species and by modifying the energy equation. Details of this work are documented by Colket, et al, 2004. and demonstrate the importance of temperature and its control to experimental programs on soot.

The model has been used also to predict particle size distributions produced by the reactor and these predictions have been compared to experimental data obtained this year. Comparisons are shown in Fig. 42 and 43. There is a dramatic contrast between the model and the experiment, with the model predicting much greater fractions of small diameter particles. A preliminary analysis of both the experiment and the model has been performed to understand the differences. It was concluded that both the model and the experiment contributed to the differences shown in Figs. 42 and 43.

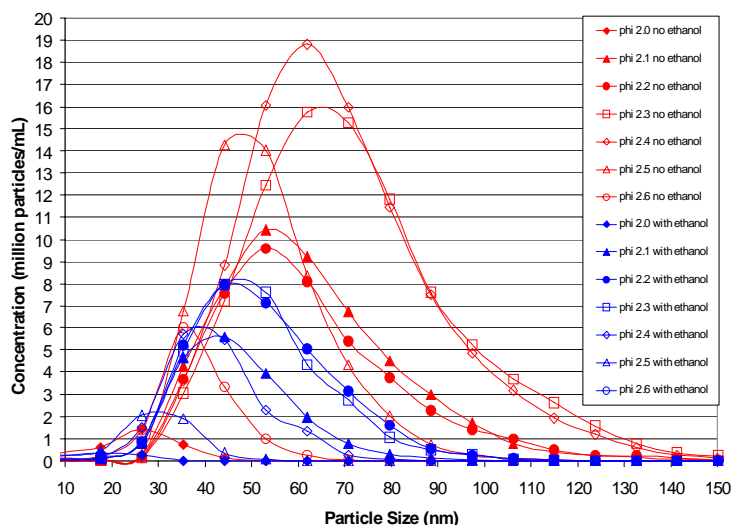


Figure 43. Experimental Particle Size Distribution for Stirred Reactor.

The model predictions of particles with sizes less than 10 nanometers were shown to be sensitive strongly to the assumed inception species. The model assumed that naphthalene was the inception species. Preliminary calculations showed that the average particle size shifted to larger values as the inception model was changed to pyrene and then to coronene. Model revisions are underway to fully incorporate these effects. In addition,

the model indicated that particle size distributions as well as soot mass were found to change as the exhaust flowed up the chimney towards the sampling probe. These effects need to be quantified in future modeling efforts.

Modeling Soot Dynamics and Sampling of Particles

The sampling process was also found to impact the experimental results. Computations using the TSI aerosol tool, showed that line loss of the small particles (< 10 nm) can be very significant. Table 6 shows results of calculations for a sample stream at nearly ambient conditions. These results are independent of number density, so dilution (which is important to minimize perturbations to particle-particle collisions) will have no effect, except to reduce the transit time to the instrumentation. The results presented in Table 6 are indicative of the significant challenges when sampling particles with small size.

Table 6. Efficiency for Transport of Particles through Sample Line without Diffusional Loss to Walls (5 lpm, 0.18” ID tube, 293K, 1 atm)

Transport		Particulate Diameter		
Length	Time	25 nm	10nm	5nm
m	sec			
1	0.2	0.98	0.94	0.86
5	1	0.93	0.8	0.6
10	2	0.75	0.68	0.45

The stirred reactor code (Colket, et al, 2004) as modified to treat oxidation rates properly (rather than empirically) and to consider non-adiabacity has been used to predict particle size distributions and number densities from the well-stirred reactor experiments. The revised analysis includes treatment of continued particle dynamics in the exhaust stream just down stream of the stirred reactor. Predicted particle sizes still were significantly smaller than that measured and reported in Reich, et al, 2003. Preliminary analysis of sample line effects were found to be significant, particularly the rapid loss to walls for particles less than 10 nm in diameter, and agglomeration effects for sample streams with number densities higher than 10⁸ #/cc. Very recent measurements by NIST (in the companion SERDP project) using a highly diluting sampling probe (~1000:1) for comparable conditions, confirm the existence of small primary particles in the exhaust stream and the sample line effects as inferred from our modeling results.

To enable better quantification of particle losses in sampling lines, we have reproduced an analysis developed by Yook and Pui [2005] and computed the size-dependent loss of particles due to diffusional, inertial, electrostatic, and thermophoretic effects. Our procedure utilizes an excel-based tool that can readily be converted to examine the performance of (i.e. losses in) a sample line. It does not account for particle coagulation, but rather is assumed that the system is diluted sufficiently to minimize such effects. Otherwise, coagulation must be treated separately. An example for sampling line conditions of 400K (gas and wall temperature), one atmosphere, 20 slpm flow, 0.533 cm tube id, and 5 meters of sample line length is given is provided in Fig 44.

For the flow parameters selected for this analysis, the electrostatic and thermophoretic penetration efficiencies are essentially unity, over most sizes of interest. The same is true

for inertial losses, at least for the sizes < 100 nm, but above particle sizes of several hundred nanometers, the inertial losses become very significant and dominating, with penetration efficiencies approaching zero for particles above one micron in diameter (1000 nm). Hence, diffusional effects dominate, as shown in Fig. 44.

Note that since these particle loss mechanisms are all first order in particle size, the computations are all independent of the particle number density. By far the dominant loss term is diffusional. Inertial effects become dominant at much larger diameters (100s of nm). These curves confirm the importance of wall losses and the likelihood that experimental particle size distributions can well be skewed, especially for particles less than 20 nm. Careful attention to sample line design and its use must be considered paramount.

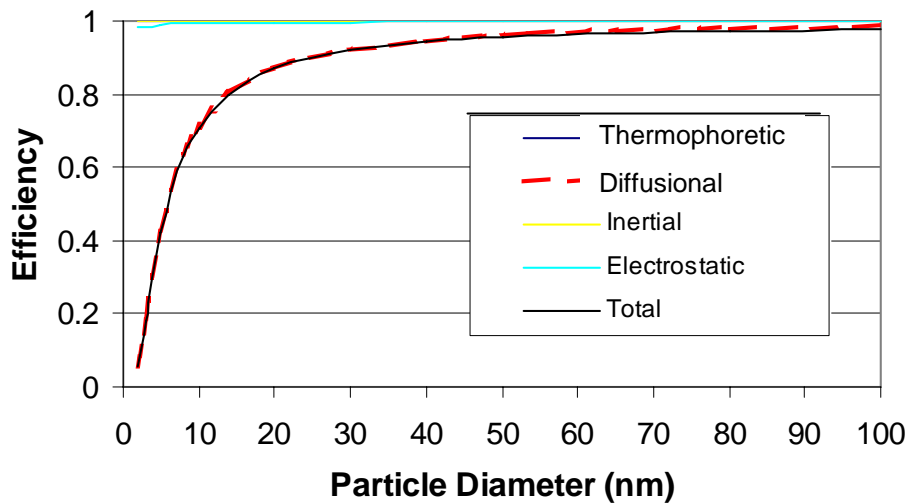


Figure 44. Computed Penetration Efficiencies of Particles through Sampling Lines.

3.2.3 Modeling of coflow diffusion flames

In a collaborative effort, soot kinetics and models as originally developed by Frenklach and coworkers (Appel, et al 2000) have been incorporated into a coflow diffusion flame code and predictions compared to experimental data and models developed by (McEnally, et al, 1998). The work has recently been published (Smooke, et al, 2004). The subroutines utilizing the Frenklach model were subsequently installed in the ‘sooting’ PSR code at UTRC and used in the present study (Colket, et al, 2004).

In related activities, a revised soot model has been developed (Smooke, et al, 2005) to quantitatively compute the changes in concentration and spatial distribution for a series of coflow flames with varying dilution ratios. The revisions included changes to the soot formation inception submodel. In addition, particle ageing effects were shown to be important and the proper treatment of optical re-adsorption was demonstrated to be important for the simulation of local flame temperatures, which in turn has a first order effect on soot formation.

4. Conclusions

The overall goal of identifying an additive that can reduce soot emissions by 70% was not achieved, without use of a metal-containing additive or with very high levels of the additive (>10% by weight). However, advances were made in the understanding or confirmation of (proposed) mechanisms for soot formation and will lead to better quantifiable tools for prediction and control of soot emissions during engine design.

Baseline studies were performed with ethanol added to ethylene, as the method and procedures could be validated against the existing experimental database. Experiments were performed in laminar premixed burner-stabilized flat flames. Soot was reduced by factors of about 50% with ethanol. Subsequent tests were performed with mixtures of heptane/toluene/ethylene to provide a better simulation of real fuel chemistry. The most significant effects were observed with a proprietary additive which apparently contains a metal. The use of metals is not perceived to be an environmentally acceptable approach. The next most effective additive is a commercial fuel additive, Kleen, which contains a variety of oxygenated (nitro) compounds. Reductions of soot emissions on the order of 30% were observed. Mixed results were obtained with pyridine, and modeling results show negligible influence of this additive. Other than for the metal-containing additive, additive concentration levels required to effect measurable reductions in soot emissions exceeded 5%.

Detailed chemical kinetic modeling supported the above experiments, but also was used to explain some unusual results obtained in the well-stirred reactor experiments using ethanol as an additive to ethylene combustion. In particular, a slight increase in soot emissions with added ethanol was explained through the dependence on temperature. In modeling these stirred reactor results, a modified code was used that fully couples the chemical kinetics and soot aerosol dynamical equations into a stirred reactor code. As part of this work, advances and demonstrations of technologies for the accurate collection of soot particles were accomplished, including probe design, sample system performance, and diagnostics.

Finally, advances to a fundamental soot formation model were accomplished by comparing simulations of coflow diffusion flames to experimental data sets. This work resulted in proposed changes to the gas-phase kinetics and soot inception models and identifying the importance of treating soot ageing and radiation losses.

References

- Appel, J., Bockhorn, H., and Frenklach, M., *Combust. Flame*, 121:122, (2000); www.me.berkeley.edu-soot-codes.f.
- Baron, P., “Aerosol Calculator”, available from pbaron@cdc.gov, Oct, 2001.
- Berry, M.V., and Percival, I.C. *Opt. Acta*, **33**, 577, (1986).
- Brocklehurst, H. T., Pridden, C. H., and Moss, J. B. (1997). “Soot Predictions within an Aero Gas Turbine Combustor Chamber”, ASME Paper 97-GT-148.
- Colket, M. B. and Hall, R. J.(1994). In Soot Formation in Combustion, H. Bockhorn, ed., Springer Verlag, Berlin, p 417.
- Colket, M. B., Hall, R. J., Stouffer, S. D., “Modeling Soot Formation in a Stirred Reactor”, Proceedings of ASME Turbo Expo 2004, Paper No. GT2004-54001, Vienna, Austria, June 14-17, 2004.
- Dalzell, W.H. and Sarofim, A.F., *A.S.M.E., J. Heat Transfer*, **91**,100 (1969).
- Dobbins, R.A. and Megaridis, C.M., *Langmuir*, **3**, 254-259, (1987)
- Frenklach, M., available: <http://www.me.berkeley.edu/soot/> December 2002.
- Frenklach, M. and Wang, H. (1991). Twenty-Third Symposium (International) on Combustion, The Combustion Institute, Pittsburgh, PA, pp. 1559 – 1566.
- Gelbard, F. and Seinfeld, J. H., (1980). *J. Coll. Int. Sci.* 78, 485.
- Glarborg, P., Kee, R. J., Grcar, J.F., and Miller, J.A.. “PSR: A Fortran Program for Modeling Well-Stirred Reactors”, Sandia Report, SAND86-8209, 1986.
- Glassman, I., Twenty-Second Symposium (International) on Combustion, The Combustion Institute, Pittsburgh, PA, p. 295, 1989.
- Hall, R.J. and Colket, M. B. (1999). “Calculations of Soot Aggregate Growth and Oxidation Using a Sectional Size Representation,” Chemical and Physical Processes of Combustion, Presentation to the Eastern States Section of The Combustion Institute, paper no. 79, North Carolina State University.
- Hall, R. J., Smooke, M. D. and Colket, M. B. (1997). Physical and Chemical Aspects of Combustion: A Tribute to Irvin Glassman, (R. F. Sawyer and F. L. Dryer, eds.) Combustion Science and Technology Book Series, Gordon and Breach, PA, pp. 189-230.

- Harris, S. J. and Weiner, A. M., *Combust. Sci. Tech.*, **32**, 267 (1983).
- Ikedo, E., Nicholls, P., and Mackie, J., *Proc. Comb Inst.* **28**, p.1709 (2000).
- Kee, R.J., Rupley, F.M., and Miller, J.A., “Chemkin-II: A Fortran Chemical Kinetics Package for the Analysis of Gas-Phase Chemical Kinetics”, Sandia National Laboratories, Albuquerque, SAND89-8009, reprinted March 1991.
- Krishnan, S.S., Lin, K.C., and Faeth, G.M., *Journal of Heat Transfer*, **123**, 332-339, 2001.
- Koylu, U. O., McEnally, C. S., Rosner, D. E., and Pfefferle, L. D., *Combustion and Flame*, **110**, 494 (1997).
- Liscinsky, D. S., Colket, M. B., Hall, R. J., Bhargava, A., True, B., and Morford, S., “Comparison of Particle Sizing Techniques in Sooting Premixed Flames”, AIAA – 2000 – 0954, *AIAA Aerospace Sciences Meeting*, Reno, NV, January 2000.
- Liscinsky, D.S., Colket, M.B., Hautman, D.J., and True, B. (2001). “Effect of Fuel Additives on Particulate Formation in Gas Turbine Combustors,” presented at the 37th AIAA/ASME/SAE/ASEE Joint Propulsion Conference, AIAA 2001-3745, Salt Lake City, Utah, July 8-11.
- McEnally, C. S., Koylu, U. O, Pfefferle, L. D., and Rosner, D. E., *Combustion and Flame*, **109**, 701(1997).
- McEnally, C. S., Schaffer, A. M., Long, M. B., Pfefferle, L. D., Smooke, M. D., Colket, M. B., and Hall, R. J., *Proceedings of the Combustion Institute*, **27**, The Combustion Institute, p. 1497, (1998) and references contained therein.
- McKinnon, J. T. and Howard, J. B. (1992). Twenty-Fourth Symposium (International) on Combustion, The Combustion Institute, Pittsburgh, PA, p. 965.
- Mackie, J. C., Colket, M. B., and Nelson, P. F., *J. Phys. Chem.*, **94**, p.4099-4106 (1990).
- Megaridis, C.M. and Dobbins, R.A, *Combust. Sci. and Tech.*, **7**, 95-109, (1990).
- Reich, R. F., Stouffer, S. D. Katta, V. R., Mayfield, H. T., Frayne, C. W., and Zelina, J., “Particulate Matter and Polycyclic Aromatic Hydrocarbon Determination using a Well-Stirred Reactor”, AIAA 2003-0664, presented at the 41st AIAA Aerospace Sciences Meeting, Jan. 6-9, 2003.
- Rosner, D.E., Mackowski, D.W., and Garcia-Ybarra, P., *Comb. Sci. and Tech.*, **80**, 87-101, (1991).
- Smooke, M. D., Hall, R. J., Colket, M. B., “Modeling The Transition From Non-Sooting To Sooting, Coflow Ethylene Diffusion Flames”, presented to the Third Joint Meeting of the U.S. Sections of The Combustion Institute, Chicago, Ill, March 15-18, 2003.

Smooke, M. D., Hall, R. J., Colket M. B., Fielding, J., Long M. B., McEnally, C. S., and Pfefferle, L. D., *Combustion Theory and Modeling*, 8, pp. 593-606, 2004.

Smooke, M. D., Long M. B., Connelly, B. C., Colket M. B., and Hall, R. J., "Soot Formation in Laminar Diffusion Flames" *Combustion and Flame*, 143, pp. 613-628, 2005.

Smooke, M. D., Long, M. B., Hall R. J., and Colket, M. B., "Computational and Experimental Study of Soot Formation in Ethylene Coflow Diffusion Flames, presented at 2005 Joint Meeting of the US Sections of the Combustion Institute Drexel University, Philadelphia, PA, March 20-23, 2005.

Stouffer, S. D., Streibich, R. C., Frayne, C. W., and Zelina, J., "Combustion Particulates Mitigation Investigations in a Well-Stirred Reactor," Paper No. AIAA 2002-3723, 38th Joint Propulsion Conference, 2002.

Strehlow, R. A., Fundamentals of Combustion, International Textbook Company, Scranton, PA, pp. 221-227, 1968.

Tein, C.L. and Lee, S.C. *Prog. Energy Combust. Sci.*, **8**, 41-59, (1982)

Tolpadi, A. K., Danis, A. M., Mongia, H. C., and Lindstedt, R. P. (1997). "Soot Modeling in Gas Turbine Combustors", ASME Paper 97-GT-149.

Waldman, L. and Schmitt, K.H. Thermophoresis and Diffusiophoresis of Aerosols. In: Aerosol Science, Chap. VI. C.N. Davies (ed.) Academic Press, London (1966).

Willeke and Baron, eds, Aerosol Measurement, Van Nostrand Reinhold, NY, (1993).

Williams, T.C., Shaddix, C.R., Jensen, K.A., and Suo-Anttila, J.M., "Measurement of the Dimensionless Extinction Coefficient of Soot within Laminar Diffusion Flames," Proceedings of the Joint Meeting of the U.S. Sections of the Combustion Institute, Philadelphia, PA, 2005.

Xu, F., Sunderland, P. B. and Faeth, G. M. "Soot Formation in Laminar Premixed Ethylene/Air Flames at Atmospheric Pressure", *Combust. Flame*, **108**, 471 – 493, 1997.

Yook, S.-J. and Pui, D. Y. U., "Estimation of Penetration Efficiencies through NASA Sampling Lines", submitted to C.-M. Lee, NASA Glenn Research Center, May, 2005.

Zhao, B., Yang, Z., Johnston, M. V., Wang, H., Wexler, A. S., Balthasar, M., and Kraft, M., *Combust. Flame* **133**, pp. 173-188, 2003.

Zhao, B., Yang, Z., Li, Z., Johnston, M. V., and Wang, H., Proceedings of the Combustion Institute, 30, The Combustion Institute, pp. 1441-1448, 2005.

Appendix - Publications/presentations from this work

Colket, M. B., Hall, R. J., Stouffer, S. D., “Modeling Soot Formation in a Stirred Reactor”, Proceedings of ASME Turbo Expo 2004, Paper No. GT2004-54001, Vienna, Austria, June 14-17, 2004.

Smooke, M. D., Hall, R. J., Colket M. B., Fielding, J., Long M. B., McEnally, C. S., and Pfefferle, L. D., *Combustion Theory and Modeling*, 8, pp. 593-606, 2004.

Smooke, M. D., Long M. B., Connelly, B. C., Colket M. B., and Hall, R. J., “Soot Formation in Laminar Diffusion Flames” *Combustion and Flame*, 143, pp. 613-628, 2005.

Wu, J., Soon, K. H., Litzinger, T., Lee, S.-Y., Santoro, R. Linevsky, M., Colket, M., and Liscinsky, D., *Combustion and Flame*, 144, pp. 675-687, 2006.

List of Symbols, Abbreviations and Acronyms

Acronyms, Abbreviations

amu	atomic mass unit
BHT	Butalyted hydroxytoluene
CHEMKIN	Software program for treating detailed chemical kinetics
CNC	Condensation Nucleii Counter
EDM	Electro Discharge Machining
EEPS	Engine Exhaust Particulate Sizer
EM	Electron Microscope
EPA	Environmental Protection Agency
HACA	Hydrogen-Acetylene-Carbon-Acetylene Soot growth mechanism
ID	Internal diameter
ISCO	
JP8	Jet Fuel
JP8+100	Jet Fuel with +100 additive package to extend heat absorption
LE	Laser Extinction
LLL	Lawrence Livermore Laboratory
MODFW	Modified Frenklach-Wang soot surface growth mechansim
NIST	National Institute of Standards and Technology
NO _x	NO + NO ₂
NoxEI	Grams of NO _x produced during combustion per kilogram of fuel
OD	Outer Diameter
OD 3	Optical Density, filter #3
PAH	Polycyclic Aromatic Hydrocarbon
P-distr	Particle size distribution
PM	Particulate matter
PM _{2.5}	Particulate matter with sizes less than 2.5 microns
PSR	Perfectly Stirred Reactor
PSU	Pennsylvannia State University
Pt	Platinum
PW	Pratt and Whitney, a division of United Technologies Corporation
Rh	Rhodium
SEM	Scanning Electron Microscope
SERDP	Strategic Environmental Research and Development
SIP	State Implementation plan
SMPS	Scannin Mobility Particle Sizer
SN	Smoke Number
STEM	Scanning Transmission Electron Microscope
TEM	Transmission Electron Microscope
TEOM	Tapered Element Oscillating Meter
TPD	Thermocouple Particle Densitometry
UTRC	United Technologies Research Center
WSR	Well Stirred Reactor

Nomenclature

A, a, b constants

d_{ev}	equivalent volume diameter
d_j	diameter of thermocouple junction
d_p	primary particle diameter
d_{aero}	aerodynamic diameter
D_f	fractal dimension
D_T	soot particle thermophoretic diffusivity
f_v	soot volume fraction (cm^3 soot/ cm^3 flame)
k_f	prefactor (constant)
k_{go}	gas thermal conductivity / T_g
I	transmitted intensity
I_o	incident intensity
L	pathlength (optical)
L_{max}	maximum distance between any two points on the perimeter of an agglomerate
m	mass of soot deposited onto thermocouple junction
n	complex refractive index
N	number density of soot particles
N_p	number of primary particles per agglomerate
Nu_j	thermocouple junction Nusselt number
T_{j0}	thermocouple junction temperature at zero insertion time
T_j	thermocouple junction temperature
T_g	local gas temperature

Greek Symbols

χ	dynamic shape factor
ϵ_j	emissivity of the thermocouple junction
ϕ	soot deposit solid fraction
λ	wavelength
σ	Stefan-Boltzmann radiation constant
σ_e	extinction coefficient